

Lipids Alter Rhodopsin Function via Ligand-like and Solvent-like Interactions

Leslie A. Salas-Estrada,¹ Nicholas Leioatts,² Tod D. Romo,³ and Alan Grossfield^{4,*}

¹Department of Biochemistry and Biophysics, University of Rochester Medical Center, Rochester, New York; ²Department of Theoretical and Computational Biophysics, Max Plank Institute for Biophysical Chemistry, Göttingen, Germany; ³Center for Integrated Research Computing, University of Rochester, Rochester, New York; and ⁴Department of Biochemistry and Biophysics, University of Rochester Medical Center, Rochester, New York

ABSTRACT Rhodopsin, a prototypical G protein-coupled receptor, is a membrane protein that can sense dim light. This highly effective photoreceptor is known to be sensitive to the composition of its lipidic environment, but the molecular mechanisms underlying this fine-tuned modulation of the receptor's function and structural stability are not fully understood. There are two competing hypotheses to explain how this occurs: 1) lipid modulation occurs via solvent-like interactions, where lipid composition controls membrane properties like hydrophobic thickness, which in turn modulate the protein's conformational equilibrium; or 2) protein-lipid interactions are ligand-like, with specific hot spots and long-lived binding events. By analyzing an ensemble of all-atom molecular dynamics simulations of five different states of rhodopsin, we show that a local ordering effect takes place in the membrane upon receptor activation. Likewise, docosahexaenoic acid acyl tails and phosphatidylethanolamine headgroups behave like weak ligands, preferentially binding to the receptor in inactive-like conformations and inducing subtle but significant structural changes.

INTRODUCTION

Lipids serve both structural and functional roles in biological membranes. They act as diffusion barriers that allow the generation of electrochemical potentials, contribute to the selectivity of external cues in signaling and provide a diverse milieu for membrane proteins (1,2). Many integral membrane proteins are sensitive to the composition of their lipid bilayers (3–8). Thus, factors that modulate the relative abundance of membrane lipids, such as dietary intake and age, can also influence the activity and organization of proteins (2,9). Alterations in the lipid composition of membranes have been linked to the onset of various pathologies, including cardiovascular diseases, obesity, cancer, and neural and retinal degeneration (10,11). Therefore, understanding the molecular basis underlying lipid modulation of membrane proteins is key for developing new and more effective therapies, targeting both membrane proteins and membrane lipids (10,12).

Lipid effects on membrane protein activity can be grouped into ligand-like and solvent-like effects (1,12). Ligand-like effects are those where lipids make specific

molecular interactions with the protein, including hydrogen bonding and charge-charge interactions (6,13,14). We define solvent-like effects as non-ligand-like effects that arise from intrinsic membrane properties, such as bilayer thickness (15–17), acyl chain order and packing (18), fluidity, curvature elastic stress (19,20), and lateral pressure (8). Due to their different natures, these effects can often be distinguished by certain characteristics of the lipids from which they originate, namely, their exchange and diffusion rates, lifetimes at the protein surface, lateral and rotational mobility, and the degree to which they require structural specificity when interacting with the protein (1,9,21). Ultimately, the relative importance of ligand-like and solvent-like lipid effects on the structure and function of a membrane protein depends on the environment and the nature of the protein itself (9,22).

G protein-coupled receptors (GPCRs) are ubiquitous seven-transmembrane (7TM) proteins whose primary function is to transduce information across lipid bilayers. They constitute the most numerous and diverse superfamily of proteins, with more than 825 distinct members identified in humans (23). Although GPCRs have a highly conserved topology, each receptor can specifically sense different external stimuli on one side of the membrane and start particular signaling responses on the other by binding a

Submitted May 26, 2017, and accepted for publication November 9, 2017.

*Correspondence: alan_grossfield@urmc.rochester.edu

Editor: Emad Tajkhorshid.

<https://doi.org/10.1016/j.bpj.2017.11.021>

© 2017 Biophysical Society.



cytosolic partner, usually a G protein (24,25). These responses mediate signaling pathways that play central roles in many physiological processes, including inflammation, vision, blood pressure, and pain (26–29). Not surprisingly, one-third to one-half of all small-molecule drugs on the market target GPCRs (30).

Lipids have been shown to influence the function and activity of GPCRs at different levels. For instance, ligand-binding affinity was found to be modulated by cholesterol in the serotonin_{1A} receptor (5-HT_{1A}R) and the chemokine receptor CXCR4; similarly, lipid headgroup composition can modulate the ligand affinity of the β_2 -adrenergic receptor (β_2 AR) (31–33). For the smoothed (Smo) receptor, cholesterol alone can act as an activating ligand and initiate signaling (34). In the cytosol, G protein recruitment and post-activation G protein subunit sorting have been observed to be sensitive to the non-lamellar-phase propensity and charge of phospholipid headgroups (35,36). Receptor dimerization and oligomerization are also thought to be tuned by direct lipid binding or by lipid-composition-dependent bilayer properties. The presence of docosahexaenoic acid (DHA), for example, modifies the rate of association of the dopamine D2 receptor and the adenosine 2A receptor (A_{2A}R), whereas palmitoylation and cholesterol also play a role in the formation of μ -opioid receptor oligomers (33,37,38).

Experimental and computational evidence have shown that GPCRs can sample ensembles of distinct conformations, which result in a broad range of signaling efficacies and functional differences (39–45). The equilibrium among these ensembles of conformations has also been proposed to be affected by the lipid composition of membranes through different mechanisms. In particular, putative cholesterol binding sites have been identified in several GPCRs, including the β_2 AR and the A_{2A}R. These non-annular cholesterol molecules are hypothesized to have allosteric and structure-stabilizing roles (46–48). Likewise, specific receptor-lipid interactions with anionic phospholipid headgroups have been proposed to stabilize the active conformation of the β_2 AR (49). Solvent-like effects have also been shown to alter the activity of these proteins, as is the case with 5-HT_{1A}R, where cholesterol-induced membrane ordering favors receptor activation (18). Given the large variety of membranes that contain GPCRs, it is not unreasonable that the vast functional diversity and specificity of these receptors may result in part from membrane-composition-dependent lipid effects.

Rhodopsin is a prototypical GPCR that mediates scotopic vision. This highly efficient photoreceptor is located in the disk membranes of the outer segment of rod cells in the retina. In its ground state (dark state), rhodopsin has negligible activity, because its covalently bound ligand, retinal, is an exceptional inverse agonist when it is in the 11-*cis* form (50). Light absorption induces the *cis*-to-*trans* isomerization of the ligand (to an agonist) and starts a relax-

ation process that drives the receptor through a series of spectroscopically distinguishable intermediates (19). This relaxation culminates when rhodopsin reaches an equilibrium between the inactive metarhodopsin I (Meta I) and active metarhodopsin II (Meta II) states. Meta II is the G protein-activating state of the receptor wherein the outer rotation of helix 6 creates a cleft at the cytoplasmic end of the protein that allows the G protein transducin to bind (51,52). The Meta I-Meta II equilibrium takes place on the millisecond timescale and has been shown to be influenced by temperature, pH, and lipidic environment (4,53). The activation process ends when retinal is hydrolyzed from the binding pocket producing ligand-free opsin and the receptor is regenerated by binding 11-*cis* retinal to restart the photocycle (54).

Rhodopsin is a good example of protein-lipid co-evolution for optimal function. The receptor constitutes ~90% of all proteins in rod outer segment (ROS) disk membranes, and the lipid composition of ROS disk membranes is highly specialized, containing a large fraction of polyunsaturated fatty acids, particularly DHA (55,56). Studies where rhodopsin was reconstituted in model membranes show that increasing concentrations of DHA enhance rhodopsin's activity (57–59) and that this effect is amplified by phosphatidylethanolamine (PE) headgroups (60). In turn, the presence of cholesterol drives the Meta I-Meta II equilibrium toward the inactive state (61). Both solvent-like and ligand-like lipid effects have been proposed to explain these phenomena (9,62–66).

Rhodopsin is sensitive to bilayer thickness, membrane order, lipid packing, and curvature elastic stress (67). Accordingly, DHA, which is known to lower the packing density and order of lipid membranes, was proposed to facilitate the conformational transitions that lead to the Meta II state, whereas cholesterol was suggested to counteract these effects by ordering the membrane and increasing its thickness (57,68). In addition, DHA and PE are non-lamellar-phase-forming lipid components and introduce negative-curvature elastic stress in membranes. Using flash photolysis experiments with different bilayer compositions, Botelho et al. (20) proposed that this so-called membrane frustration might be relieved by the transition to Meta II. Although sophisticated in its conception, this and other models arguing in favor of solvent-like lipid effects do not take into account the heterogeneity of the hydrophobic surface of the protein and the distinct characteristics of the lipids that are close or far from the receptor (69). For instance, PE has hydrogen-bonding capacity, whereas the multiple double bonds of DHA can form π - π stacking interactions with aromatic side chains and the remaining single bonds have low isomerization energy barriers that make them extremely flexible and could potentially facilitate protein-lipid interactions (60,70,71). Indeed, saturation-transfer NMR experiments have shown that lipids directly associate with rhodopsin and behave as weak ligands (65,69).

However, the exact molecular details of these putative protein-lipid interactions are still largely unknown.

Here, we investigate the role of lipid membranes in modulating rhodopsin's structure and dynamics at atomic resolution. We present an ensemble of multi-microsecond all-atom simulations of rhodopsin along its photocycle embedded in 1-stearoyl-2-docosahexaenoyl-*sn*-glycero-3-phosphatidylethanolamine (SDPE) membranes. Our analysis of the resulting trajectories suggests that membrane modulation of rhodopsin activity is due to both solvent-like and ligand-like properties of lipids and that these effects are state dependent.

METHODS

System construction

Crystal structures have been solved for bovine rhodopsin in the dark state (72), Meta II (52), and opsin (73) (PDB: 1U19, 3PXO, and 3CAP, respectively). We used these structures as the starting points of four of our systems, including dark-state rhodopsin with retinal removed (hereafter referred to as dark opsin). Opson exists in an equilibrium between inactive-like and active-like receptor conformations. It was crystallized in low-pH conditions and has a C_{α} root mean-square deviation of 0.51 and 2.8 Å with respect to the Meta II and dark-state structures, respectively (52,72,73). However, at pH ~6.1, its Fourier transform infrared spectrum closely resembles that of the dark state, and the apo protein can activate transducin only very poorly (50). Therefore, we consider dark opsin a model for the hypothesized inactive-like opson structure.

The starting structure of the Meta I state was obtained from previous simulation work in which the protein was initialized and equilibrated in the dark state and retinal isomerization was accomplished by applying an external potential on the C10-C11=C12-C13 torsion (74). This model of Meta I formation emulates the complex counterion hypothesis formulated by Lüdeke et al. (75) and was validated by direct comparison of the ^2H NMR spectra of retinal's methyl groups calculated from simulation and measured experimentally (74).

We built six independent replicates of each of the five protein structures, for a total of 30 trajectories and ~163 μs of simulation time. In each system, the receptor was embedded in a lipid bilayer composed of 123 SDPE molecules. These phospholipids contain a PE headgroup, an 18-carbon saturated stearoyl (STEA) chain and an ω 3 22-carbon DHA chain with six double bonds. ROS membranes are highly enriched in DHA (~35–60% of all phospholipid acyl tails), whereas PE constitutes ~40% of all headgroups. Hence, we chose SDPE as a simplified approximation of rhodopsin's lipid environment. Experimental work with pure SDPE bilayers is challenging, since these lipids are not only susceptible to oxidation, but also tend to form an inverse hexagonal (H_{II}) phase at physiological temperatures (293–323 K), as repeatedly shown by NMR spectroscopy and x-ray diffraction (76,77). In practice, SDPE is often titrated in with other lipids like 1-palmitoyl-2-oleoyl-*sn*-glycero-3-phosphatidylcholine, whose spontaneous monolayer curvatures are not as extreme (70). However, this phase transition does not occur on the timescale of our simulations. Our choice of membrane takes into consideration that the presence of a second lipid species necessarily introduces lateral membrane-reorganization degrees of freedom, which have timescales of hundreds of nanoseconds to microseconds (78–80). It also reflects that any lipid modulation effects are to be more cleanly discernible if the Meta I-Meta II equilibrium is shifted in a single direction, as is the case for DHA and PE, which favor the active state of the receptor (57). These membranes were constructed according to a procedure analogous to that described by Grossfield et al. (45,79,81), fully hydrated with ~8000 waters, and embedded in 74 Å × 74 Å × 90 Å periodic boxes with 100 mM NaCl (in addition to neutralizing salt). Total system sizes were ~46,000 atoms. Because the coordinates of the non-protein components

of the system are randomized during construction, this approach ensures that every replicate is as independent as possible, with the only caveat being that the same initial protein structure must be used. This protocol has been recently implemented as an automated membrane-building tool in LOOS, a Python/C++ open-source library for molecular dynamics (MD) analysis (82).

Simulation details

We ran these simulations using the NAMD simulation package (version 2.8) (83) with the CHARMM22 force field with CMAP corrections for protein parameters (84,85) and the CHARMM36 force field for lipid parameters (86). 11-*cis* and all-*trans* retinal parameters were kindly provided by Dr. Scott Feller (87). The systems were energy minimized and initially equilibrated for ~10 ns in the NP γ T ensemble. We have found that using a constant lateral surface area as part of energy minimization helps to stabilize the volume of the simulation box, allowing the water in the bulk region to equilibrate. Production was carried out in the NP γ T ensemble, with $\gamma = 30$ dyn/cm (see Supporting Material, Section S1, for further details). The pressure (1 bar) was regulated using a Langevin piston with an oscillation period of 200 ns and a damping timescale of 100 ns, whereas the temperature (310.15 K) was controlled using a Langevin thermostat with a damping coefficient of 2 ps⁻¹. We used the Velocity Verlet integrator with a 2 fs timestep and the SHAKE algorithm to constrain hydrogen-containing bonds (88). For the treatment of long-range electrostatics, we employed the smooth particle-mesh Ewald (PME) summation method (89) with a cutoff of 10 Å and a grid of 75 × 75 × 96 points (~1 Å/grid point). All simulations were run on the BlueGene/Q supercomputer of the Center for Integrated Research Computing (CIRC) at the University of Rochester.

Simulation analysis

Analysis was performed with the trajectories sampled at 1 ns resolution (except as indicated), with the first 500 ns excluded to allow the protein and membrane to relax. Unless explicitly noted, we used either existing analysis tools included in the current LOOS distribution (version 2.3.1) (82) or in-house code generated using LOOS. The source code for LOOS is available for download at GitHub (<http://github.com/GrossfieldLab/loos>). Trajectory visualization, image rendering and data plotting were carried out using VMD (version 1.9.2) (90), PyMOL (version 1.8.0.0) (91), and gnuplot (version 5.0, www.gnuplot.info). We refer the reader to the Supporting Material for an extensive description of the analysis mentioned in the main text.

RESULTS

We examined the possibility that lipids could affect rhodopsin's function by differently modulating the receptor along its photocycle via solvent-like or ligand-like effects. We carried out extensive simulations of rhodopsin in SDPE membranes with starting structures corresponding to the dark state, Meta I, Meta II, opsin, and dark opsin (an apo dark-like state; see Methods for details). The aggregate data set (~163 μs) included six independently constructed replicates of each protein state that we used to assess the statistical significance of our observations.

Changes in membrane structure during rhodopsin activation

Reconstitution experiments of rhodopsin in different membrane compositions have shown that the presence of

PE headgroups and DHA acyl chains favors rhodopsin activation (3,57). This effect has been proposed to be the result of curvature elastic stress in the membrane coupled with changes in the shape of the receptor during activation (19,20,92). To examine any changes in the shape of the protein in the context of our simulations, we computed the cross-sectional area of the receptor for the dark, Meta I, and Meta II states, which are part of rhodopsin's activation process. Briefly, we sliced the systems into thin sections along the membrane normal that were partitioned using a Voronoi decomposition in the plane of the membrane. The cross-sectional area of each thin slice was taken as the smallest convex hull delimiting the atoms of the protein (see *Supporting Material*, Section S2, for further details). Figs. 1 and S2 show the average cross-sectional areas of rhodopsin along the bilayer normal computed from the dark-state, Meta I, and Meta II systems. Our simulations reveal small changes in the transmembrane region of the protein, wherein the receptor undergoes a decrease in cross-sectional area ($-15 < z < 15$; Fig. 1, inset) and appears to be slightly (but significantly) more elongated in the Meta II state. Treating the individual trajectories as single measurements, we were able to calculate accurate error bars and also determine whether the noted changes are statistically significant (see Figs. 1 and S2, b-d).

To understand the effects of these local changes in cross-sectional area, we studied the organization and structure of the lipids surrounding the receptor. Experimentally, ^2H quadripolar splittings measured via NMR provide a way to quantify the average orientations sampled by C-D bonds with respect to the membrane normal along perdeuterated

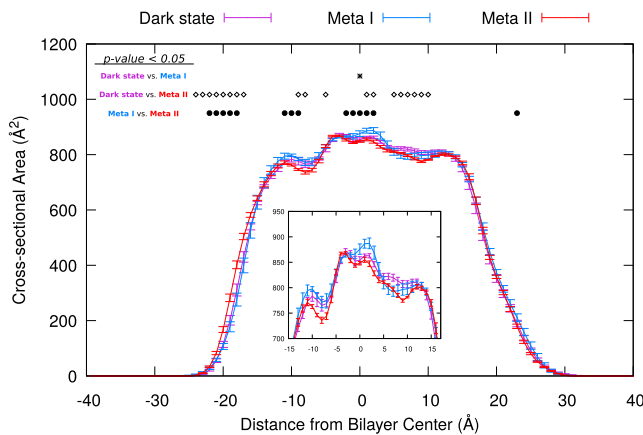


FIGURE 1 Cross-sectional area of rhodopsin during activation. Average cross-sectional area profiles of rhodopsin states are calculated from six trajectories per protein state. Error bars indicate the mean \pm SE, computed by treating each simulation as a single data point. Significantly different cross-sectional areas among protein states ($p < 0.05$) were determined with a *t*-test for each pairwise comparison and are annotated at the top by stars (dark state versus Meta I), open diamonds (dark state versus Meta II), and dots (Meta I versus Meta II). The inset corresponds to the cross-sectional areas of the $-15 < z < 15$ region, with the y axis scaled up. To see this figure in color, go online.

fatty acid tails (93). This observable is customarily referred to as C-D bond order parameters and is used to gauge membrane disorder and assess the average structure of lipid bilayers. We investigated activation-induced changes in local membrane disorder by computing a whole-chain analog of C-D bond order parameters (hereafter molecular order parameters), where the angle between the second or third principal axes of phospholipid acyl chains and the membrane normal is averaged instead (see *Supporting Material*, Section S3, for details).

We calculated the molecular order parameters of DHA and STEA acyl chains as a function of distance from the receptor to track down changes in the structure of the bilayer during rhodopsin activation. At $11\text{--}15 \text{ \AA}$ from the centroid of the protein, we observe that where STEA order is reduced compared to the distal region of the membrane ($>25 \text{ \AA}$) in the dark and Meta I states, it is slightly increased in the case of Meta II (Fig. 2 a). These differences in STEA molecular order parameters between the inactive (dark and Meta I states) and active (Meta II state) distributions are statistically significant in this region of the membrane (Fig. S3). A lower molecular order parameter is indicative of either increased chain disorder or systematic tilting of the chain. Therefore, our analysis of the dark-state, Meta I, and Meta II trajectories suggests that there is a local ordering effect in the lipids surrounding the receptor upon activation, wherein STEA acyl chains become more ordered around the protein. This observation is further supported by the

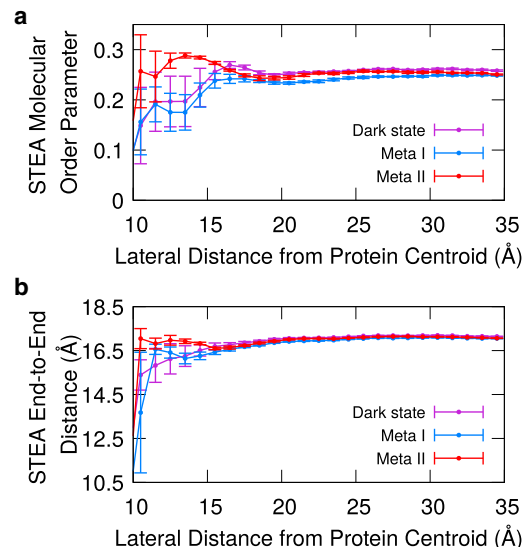


FIGURE 2 Activation-induced changes in the structure of the membrane. (a) Average distributions of molecular order parameters of STEA acyl chains as a function of distance from the protein centroid are shown. (b) Average distributions of STEA end-to-end distances as a function of distance from the protein centroid computed from atoms C1 and C18 of the acyl chain are shown. These averages were computed from the distributions of six trajectories per protein state. Error bars indicate the mean \pm SE, calculated by treating each trajectory as a single data point. To see this figure in color, go online.

distribution of end-to-end distances of STEA acyl chains as a function of distance from the protein, which shows that these fatty acids are in more stretched conformations near the receptor in the Meta II state compared to the dark or Meta I states (Fig. 2 b). Taken together, these results suggest that when the transmembrane region of the protein gets elongated upon activation, the lipid tails in the vicinity of the protein ($\sim 11\text{--}15$ Å from the protein centroid) can compensate for the resulting hydrophobic mismatch by adopting more stretched conformations. This end-to-end elongation of the acyl chains in Meta II brings about a local ordering of the membrane that is not present in the dark state or Meta I (Fig. 2). The decrease in the receptor's cross-sectional area in Meta II, which occurs mainly in the hydrocarbon region (Fig. S2), could also facilitate these changes in the structure of the membrane.

State dependence of lipid-binding lifetimes

Differences in the structure and distribution of phospholipids surrounding the receptor during activation may also modulate direct interactions between rhodopsin and annular or non-annular lipids. In previous work, we had identified regions on the protein surface that are likely to be enriched in tight-packing lipid events (79). Here, with the benefit of far longer simulations in different functional states, we identified lipids that form long-lived interactions where the chains intercalate themselves between the helices. To determine whether these interactions are state dependent, we monitored the lifetimes of lipid-binding events in rhodopsin simulations starting from different functional states. For the purpose of our analysis, we reasoned that instances of fatty acid tails penetrating the helical bundle, as opposed to acyl chains just contacting the surface of the protein, would be more stable and more clearly discernible. For this reason, lipid-binding events were defined by the presence of one or more lipid heavy atoms inside the protein core at a given time point. To discriminate the interior from the exterior of the protein, we again took thin slices of the receptor along the membrane normal and applied a Voronoi analysis, using only the geometric centroids of the receptor's transmembrane helices to define convex hulls (see Figs. 3, S4, and S5, and refer to [Supporting Material](#), Section S5, for further details).

Fig. S4 shows the distributions of residence times of DHA and STEA binding events computed from the full trajectories. The total number of DHA penetration events was larger than the total number of STEA penetration events for every protein state. This result is consistent with previous work suggesting that DHA is enriched at the surface of the receptor and can penetrate deeper than STEA into rhodopsin's core (63,79,94). Since long-lived binding events are more likely to have ligand-like effects and induce changes in the protein, we examined the possibility that the observed preference for DHA translated to

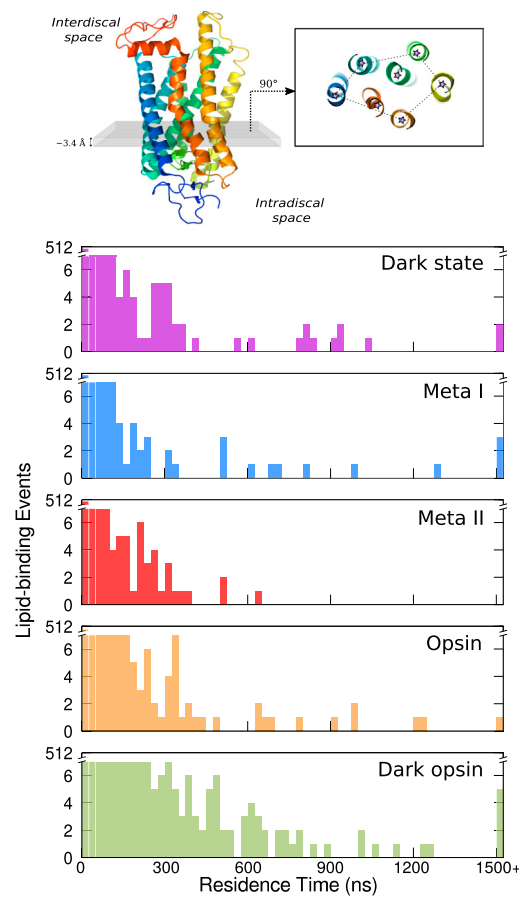


FIGURE 3 Residence times of DHA acyl chains inside rhodopsin. Top: Scheme illustrating the approach we employed to quantify DHA-binding events in our simulations is shown. Briefly, we took thin slices of the system along the membrane normal and used a Voronoi analysis to find the smallest convex hull containing all transmembrane helices in a slice. We counted a DHA tail as being inside the protein if one or more of its heavy atoms was inside any of these convex hulls. Bottom: Distributions of the residence times of DHA-binding events by protein state computed from the full trajectories (including the first 500 ns of the simulation). Binding events >1500 ns are grouped together. To see this figure in color, go online.

longer residence times for this fatty acid inside the receptor. There were at least 1.7 times more long-lived DHA binding events (those lasting >500 ns) than STEA binding events in each protein state, suggesting that DHA-rhodopsin interactions are more stable. The vast majority of the long-lived DHA penetration events occurred when the protein was in inactive-like states—dark, Meta I, or dark opsin—as well as in one opsin trajectory that spontaneously deactivated ~ 550 ns into the simulation (Fig. 3). To assess the statistical significance of these observations, we performed a *t*-test to compare the number of total, short-lived (<20 ns), and long-lived DHA penetration events per microsecond of simulation time among protein states. Interestingly, although the number of total and short-lived events per microsecond was not significantly different between active-like and inactive-like protein states ($p > 0.05$), the number of long-lived events in the

dark-state, Meta I, and dark-opsin trajectories were significantly different ($p < 0.05$) from the ones found in the Meta II simulations. We repeated these calculations excluding the first 500 ns and the first microsecond from the simulations (see Fig. S5). Although the number of lipid penetrations varied in each case, the differences between the inactive and active states in terms of their observed long-lived binding events are robust. Overall, these results suggest that DHA interacts with rhodopsin in a state- and conformation-dependent manner.

Ligand-like effects of DHA on protein structure and ligand behavior

The premise that DHA-rhodopsin interactions might be state dependent prompted us to investigate the possible origins of this preference. It has been previously proposed that the intrinsic geometry of a given protein state might be better suited to accommodate particular lipid species, such as DHA (70). Another possibility is that specific regions or specific residues on the protein surface differentially associate with lipids in active-like and inactive-like conformations of the receptor, depending on their accessibility and availability for binding (63,67).

To test the latter hypothesis, we investigated whether there were also significant differences among states regarding protein residues involved in DHA-binding events. Specifically, we computed the likelihood for a given residue to make contact with DHA (see [Supporting Material](#), Section S6, for further details). For our six replicates per protein state, we calculated the fraction of simulation time that each protein residue was in contact with any given DHA acyl chain and normalized this quantity by the length of the trajectory. Using these results, we carried out a *t*-test to find which residues were occupied by DHA at significantly different rates in the five protein states, comparing two states at a time. A table with these comparisons is shown in Fig. S6. For the dark state and Meta II (which can be thought of as the end points of the rhodopsin activity spectrum), these residues are mapped in sphere representation onto the dark-state crystal structure (PDB: 1U19 (72)) in Fig. 4. Residues with higher occupancies (i.e., normalized fraction of simulation time in contact with DHA) in the dark state are colored purple, whereas residues with higher occupancies in Meta II are colored red. For clarity, residues with small overall occupancies are not shown, even if the differences between protein states are statistically significant. Unsurprisingly, most of the residues are located in the interface of helices 5 and 6 and the interdiscal end of helix 7, where the largest conformational changes occur during activation.

Residue F212, or 5.47 in Ballesteros-Weinstein notation (95), is found in the middle section of helix 5 and spends significantly more time in contact with DHA when the pro-

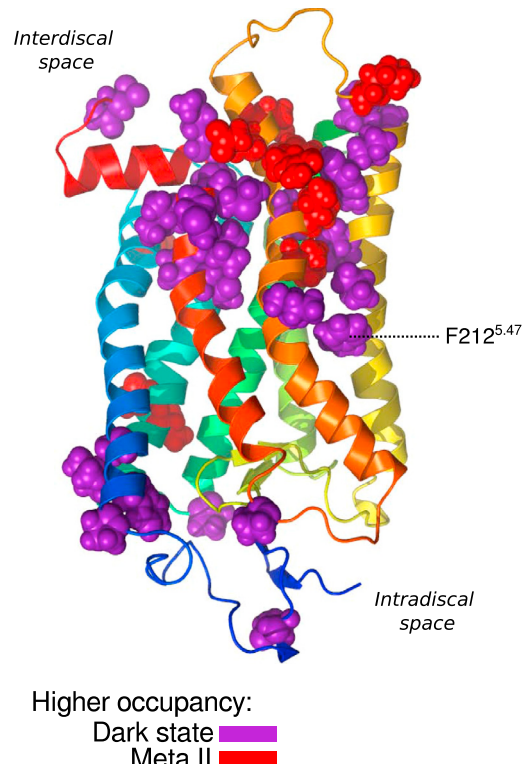


FIGURE 4 Protein residues with significantly different DHA occupancies in the dark state and Meta II. Amino acids that spent significantly different simulation times (on average) in contact with DHA in either the dark state or the Meta II trajectories are shown in sphere representation. Significance was judged as $p < 0.05$, using six trajectories per protein state as single measurements for the calculation. To see this figure in color, go online.

tein is in the dark state (65% of the simulation time) than when it is in Meta II (21% of the simulation time). Fig. 5 *a* shows a direct interaction between a DHA acyl chain and this residue in one of our dark-state trajectories, as defined by the minimum interatomic distance between the two. In the simulation, F212^{5.47} undergoes a rotameric switch when the DHA tail of the phospholipid binds between helices 5 and 6 (Fig. 5, *a* and *b*, ~950 ns). This is not an isolated event; indeed, the rate of F212^{5.47} isomerization was at least 1.5 times higher in the dark-state trajectories than in Meta II.

Evidence from previous simulation work and NMR experiments shows that polyunsaturated acyl chains have a strong preference for aromatic amino acid residues due to interactions between the double bonds in the hydrocarbon tails and aromatic side chains, and that these interactions seem to be largely non-specific (63,67,71). Notably, rhodopsin's ligand-binding site is lined by several aromatic residues that directly interact with the hydrophobic ligand (96). For instance, F212^{5.47} is positioned within ~5–7 Å of retinal's β -ionone ring (97). Therefore, we hypothesized that the isomerizations of some of these aromatic residues induced by DHA binding could propagate to the ligand,

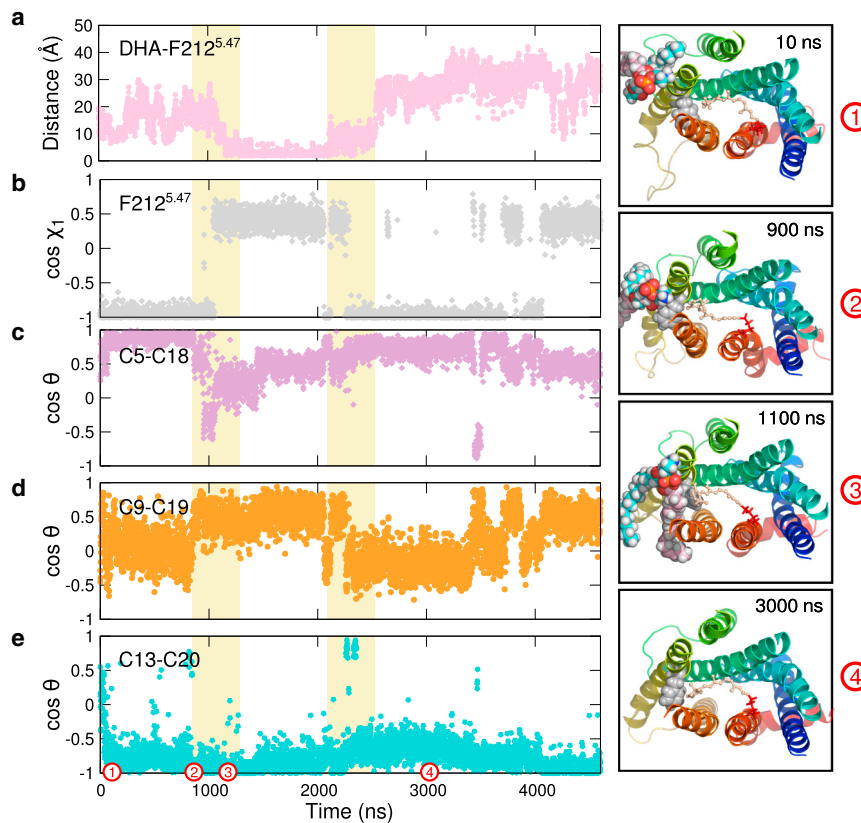


FIGURE 5 Direct DHA-rhodopsin interactions can alter the orientations of aromatic side chains and retinal methyl groups. (a) Time series of the minimum heavy-atom-to-heavy-atom distance between a DHA acyl chain and protein residue F212^{5,47} in one of the dark-state trajectories. (b) Time series of the χ_1 torsion angle of F212^{5,47} computed from the same dark-state trajectory as in (a). (c–e) Retinal methyl orientations as a function of simulation time computed from the same trajectory as in (a) and (b): (c) C5-methyl (C5-C18), (d) C9-methyl (C9-C19), and (e) C13-methyl (C13-C20). Right column: Time stills showing rhodopsin viewed from the intradiscal side of the membrane in cartoon representation (only TM segments are shown for clarity). K296^{7,43} and retinal are shown in stick representation. An SDPE phospholipid is drawn in sphere representation. To see this figure in color, go online.

altering its orientation. To test this, we monitored the orientations of the three methyl groups of retinal, as described by Leioatts et al. (45). Briefly, we tracked the vector orientations between retinal atom pairs C5-C18, C9-C19, and C13-C20 with respect to the membrane normal as a function of simulation time (see Supporting Material, Section S7, for further details). Fig. 5, c–e, shows time series of retinal methyl-group orientations computed from the same dark-state trajectory as in Fig. 5, a and b. There, retinal orientation is concomitantly altered with the torsion angle of F212^{5,47}.

Although Fig. 5 focuses on a single event in one trajectory, we observed other instances of coupling between changes in the orientation of retinal's methyl groups, the torsion angles of aromatic amino acids and the formation/breakage of interactions between these residues and DHA acyl chains. This was especially the case for F212^{5,47}, W265^{6,46}, and Y268^{6,51}, which account for ~30% of the ligand's binding pocket in the ground state (24). When we histogrammed the observed retinal methyl orientations in the dark state and averaged the resulting distributions of our six trajectories, we found that the three methyl groups sampled a wide range of orientations (Fig. 6), suggesting that long-lived interactions between DHA and aromatic residues are at least partially responsible for alterations in the orientation of the ligand.

PE headgroups alter the conformation of intracellular loop 3

Intracellular loop 3 (ICL3) of rhodopsin connects helices 5 and 6 at the cytoplasmic side of the receptor and has been implicated in protein-protein interactions with transducin,

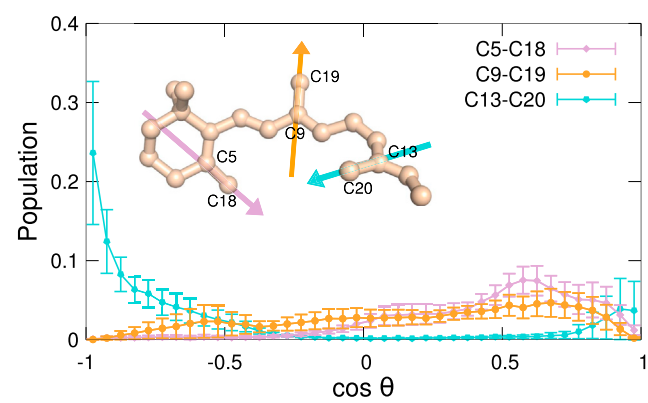


FIGURE 6 Retinal methyl orientations in dark-state rhodopsin. Average distributions of the orientations sampled by retinal methyl groups: C5-methyl (C5-C18), C9-methyl (C9-C19), and C13-methyl (C13-C20) are shown. $\cos \theta = 1$ means that the vector is parallel to the membrane normal (i.e., pointing toward the interdiscal/intracellular side); and $\cos \theta = -1$ indicates that it is anti-parallel to the membrane normal (i.e., pointing toward the intradiscal/extracellular side). Error bars indicate the mean \pm SE of six trajectories. To see this figure in color, go online.

rhodopsin kinase, and arrestin (98–102). This region possesses intrinsic structural plasticity, as evidenced by its high B-factors and lack of electron density in some dark-state crystal structures; in other GPCRs, it must be truncated or artificially stabilized by a fusion protein for crystallization to occur (103,104). Our simulations suggest that this protein region is also altered by direct protein-lipid interactions. From crystal structures of the active state, ICL3 is known to become partially structured upon activation (52,73). However, we observed that the loop can acquire some degree of partial structuring even when the receptor is in inactive-like protein states (dark state, Meta I, and dark opsin).

Fig. 7 a shows the secondary structure assignments of residues Q225^{5,60}–V250^{6,33} computed from one of the dark-state trajectories (see **Supporting Material**, Section S9, for details). A salt bridge between E232^{5,67} and K248^{6,31} breaks concomitantly with ICL3 gaining helical structure (**Fig. 7 b**). Surprisingly, we found that this interaction is bridged and then disrupted by PE headgroups (**Fig. 7, bottom row**). The amino group of PE forms a hydrogen bond with the side chain of E232^{5,67}, displacing K248^{6,31}, whereas K248^{6,31} hydrogen-bonds with PE's phosphate group (**Fig. 7 c**); similar behavior was observed in five of the six dark-state trajectories. Although **Fig. 7** shows a single trajectory, we consistently saw ICL3 undergoing a conformational change and PE bridging the interaction between E232^{5,67} and K248^{6,31} in the dark-state (**Fig. S7**), Meta I, and dark-opsin simulations. The resulting helix varied in length and starting position. Its average length was 5.2 ± 0.5 residues over the three inactive-like protein states, with residues 233–235 forming the central part of the resulting secondary structure. These observations suggest that PE headgroups favor the open state of the salt bridge and stabilize the partial structuring of ICL3 in inactive-like protein states, and they further support the

view that rhodopsin structure can be modulated by direct protein-lipid interactions in a conformation-dependent manner.

DISCUSSION

MD simulations have been used in the past to examine protein-lipid interactions in rhodopsin systems (63,64,79). However, most of this work predated the crystal structure of Meta II (52) and, due to the computational power available at the time, was limited to the nanosecond timescale. The work presented here extends previous analysis to include multiple protein states and longer simulation times. Generally, GPCR state transitions have remained elusive for unbiased simulations with standard force fields, given their intrinsic timescales (105). We take advantage of the existing number of rhodopsin structures in multiple states and prior simulations to study the effects of lipids along its photocycle.

Our analysis of the dark, Meta I, and Meta II states suggests that activation-related conformational changes in the receptor are coupled with changes in the structure of the bilayer. We note that there is an elongation of the transmembrane region of the protein in the Meta II state (**Fig. 1**) that seemingly increases the hydrophobic surface of the protein, particularly on the intradiscal side of the membrane. We also note that STEA acyl chains are more ordered around the protein (~ 11 – 15 Å from the centroid of the receptor) in the Meta II state than in the dark or Meta I states (**Fig. 2 a**). Our results suggest that this local ordering effect is likely to be associated with the stretching of these fatty acid tails that occurs in that area of the membrane in the active state (**Fig. 2 b**), perhaps in an effort to compensate for the changes in the conformation of the protein. These observations support the view that rhodopsin activation

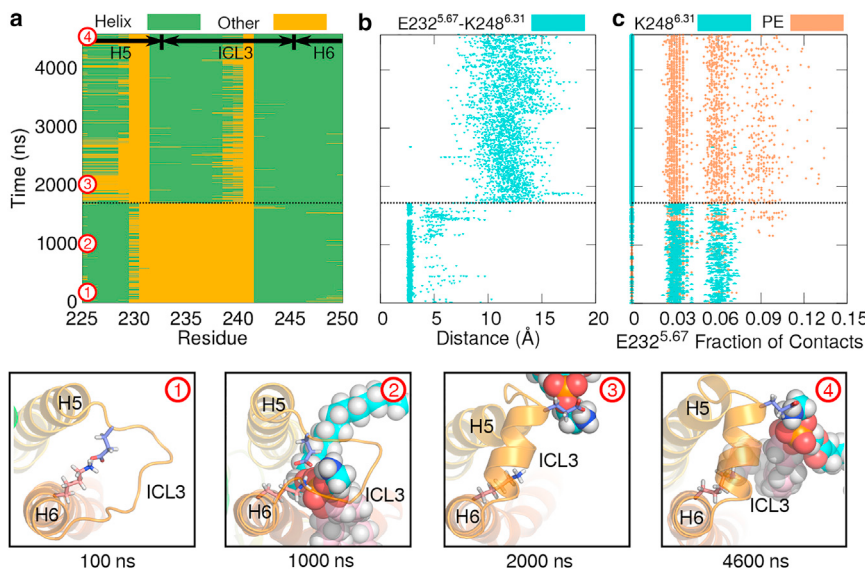


FIGURE 7 ICL3 samples multiple conformations in inactive-like rhodopsin. **(a)** Time course of secondary structure assignments of protein residues Q225^{5,60}–V250^{6,33} in one of the dark-state trajectories is shown. ICL3 partially turns into a helix ~ 1700 ns into the simulation. **(b)** Time course of the minimum distance between E232^{5,67} and K248^{6,31} computed from the same dark-state trajectory as in **(a)**. **(c)** Fraction of contacts between E232^{5,67} and K248^{6,31} or PE headgroups computed from the same trajectory are shown. The fraction of contacts between PE and E232^{5,67} increases concomitantly with the breakage of the E232^{5,67}–K248^{6,31} salt bridge and ICL3 structuring. Bottom row: Conformation of ICL3 at different time points of the same trajectory, seen from the cytoplasmic side of the receptor. E232^{5,67} and K248^{6,31} are shown in stick representation. SDPE phospholipids located within 3.2 Å of E232^{5,67} are shown in sphere representation. To see this figure in color, go online.

induces hydrophobic mismatch at the membrane-water interface (16,106), and they agree with the model proposed by Botelho et al. (20), which suggests that this activation-induced mismatch promotes stretching in the membrane, which in turn could reduce the curvature stress of the bilayer. Moreover, in the case of the dark state and Meta I systems, where the membrane is not as ordered around the protein, it is likely that DHA acyl chains may move more freely, conceivably facilitating direct interactions with the protein, as suggested by Fig. 3.

Because of their extreme flexibility, DHA acyl chains increase the fluidity of lipid membranes (68). Thus, bilayers containing high concentrations of DHA tend to be more loosely packed and less ordered. This effect, which is particularly enhanced at the annular region of certain proteins, such as the 5'-nucleotidase and the Mg²⁺-ATPase, is thought to be responsible for increasing membrane protein activity by allowing proteins greater mobility (5). In the case of rhodopsin, evidence from ultraviolet-visible spectroscopy indicates that the presence of these polyunsaturated lipids shifts the Meta I-Meta II equilibrium toward Meta II (4). Several lines of investigation, including solid-state NMR, FRET, and MD simulations, have shown that there is a strong preference for DHA, as compared to other lipid species, to accumulate at the lipid-protein interface of rhodopsin (63,64,69,79,107,108). Based on this work, it was previously suggested that the ability of DHA to more deeply penetrate the receptor's core may also have functionally relevant implications in rhodopsin activation (63,94). Our results suggest that DHA may behave as a weak ligand with multiple low-affinity binding sites (Figs. 3 and 4). This view is consistent with saturation-transfer NMR experiments, where the effect of titrating DHA in rhodopsin-containing reconstituted membranes was fit to a ligand-binding model with ~16 binding sites (69).

Our simulations also suggest that DHA interacts with rhodopsin in a state-dependent manner and that it associates differently with inactive-like and active-like protein states (Fig. 3), which is a necessary feature of allosteric modulation of function. Specifically, we found that DHA has a larger number of long-lived binding events in inactive-like protein states (dark, Meta I, and dark opsin). Botelho et al. (20) suggested that non-lamellar-phase-forming lipids, such as DHA, stabilize the Meta II state by introducing curvature elastic stress in the membrane (a solvent-like lipid effect). Our data support a complementary destabilizing role for DHA, where these polyunsaturated fatty acids preferentially bind inactive-like protein states and potentially disrupt stabilizing interactions within the receptor (a ligand-like lipid effect) (66). Indeed, the presence of these polyunsaturated acyl chains has been shown to decrease the stability of the receptor (61,107), although separating the role of lipid-protein effects from those due to the lower T_m of polyunsaturated lipid membranes is problematic.

Spontaneous *cis*-to-*trans* isomerization of rhodopsin-bound retinal is on the order of 10⁻⁸ s⁻¹, owing to a photoactivation energy of ~48 kcal/mol (109,110). For isolated retinal, however, this energy barrier is significantly lower (~14.9 kcal/mol) (111). This discrepancy suggests that rhodopsin dramatically reduces the rate of retinal isomerization caused by thermal noise, which is important for achieving a high signal/noise ratio in dim-light conditions. Within the binding pocket, retinal's Schiff base and its counterion (E113^{3,28}) form a stabilizing salt-bridge interaction, but the ligand is also tightly packed and its mobility is hindered by steric constraints (96). Unexpectedly, we observed that 11-*cis* retinal sampled a broad distribution of orientations in the dark-state simulations (Fig. 6). Our analysis of these trajectories and the long-lived DHA-binding events that we observed in them (e.g., Fig. 5) suggests that direct protein-lipid interactions are at least partially responsible for these broad distributions of orientations and supports the possibility of a destabilizing role for DHA in inactive-like protein conformations.

Other direct protein-lipid interactions can also modulate rhodopsin's conformational ensemble (12,112). Protein residues at the ends of transmembrane helices can often satisfy their own hydrogen-bond requirements with lipid headgroups (12). Our simulations suggest that the hydrogen-bonding ability of PE headgroups can favor the formation of secondary structure in rhodopsin's ICL3. These findings illustrate the structural plasticity of this region and help reconcile the different ICL3 conformations observed in existing dark-state crystal structures (72,113,114). Our dark-state trajectories were initialized from the tetragonal P4₁ crystal structure solved by Okada et al. (72) (PDB: 1U19), in which ICL3 is entirely unstructured. During the simulations, ICL3 sampled an ensemble of conformations that included an additional helical turn at the end of helix 5 (Figs. 7 and S7), as observed in the trigonal P3₁ crystal structure solved by Li et al. (113) (PDB: 1GZM). PDB: 1GZM has been suggested to adopt a more native-like conformation than PDB: 1U19 in this region (115,116). Interestingly, ICL3 stays unstructured in simulations of the dark state embedded in 1,2-dimyristoyl-sn-glycero-3-phosphatidylcholine (DMPC) bilayers (117). DMPC phospholipids contain two short, saturated myristoyl acyl chains and a phosphatidylcholine headgroup, which cannot hydrogen bond. In these membranes and in the absence of a Gα-derived peptide, the loop swiftly becomes disordered (<200 ns) in multiple trajectories even when started from the active state, where helix 5 is elongated (117). This result is consistent with experimental evidence showing that rhodopsin is largely inactive in DMPC membranes (19,57,118). Conversely, ICL3 remains very close to its initial conformation when active-like (Meta II and opsin) in our simulations with SDPE membranes, suggesting that the lipid environment of the receptor contributes to modulating the conformations accessible to this protein region.

CONCLUSIONS

Is the lipid control of rhodopsin's function a ligand-like effect or a solvent-like effect? Our analysis suggests that the answer is Yes. These are often presented as mutually exclusive hypotheses, but this work demonstrates that both phenomena are present in rhodopsin systems. In our simulations, activation-induced changes in the structure of the receptor were coupled to changes in the structure of the membrane. Specifically, we observed an increase in the local order and effective length of STEA acyl chains in the vicinity of the protein. On the other hand, our data also suggest that direct protein-lipid interactions may play important roles in modulating rhodopsin structure and that these contributions are state dependent. For instance, we found that DHA acyl chains can bind to the receptor preferentially to inactive-like protein conformations, acting as a weak ligand; likewise, direct interactions between rhodopsin and PE headgroups seemed to stabilize the partial structuring of ICL3 in inactive-like protein states.

Given the current difficulties in capturing GPCR state transitions using all-atom unbiased MD, simulating five different functional states along rhodopsin's photocycle allowed us to study different mechanisms by which the receptor interacts with its surrounding membrane in each protein state. Multiple replicates corresponding to each of these states were required to assess the significance of our observations. Our work emphasizes the value of the high level of detail provided by all-atom simulations in hypothesis testing and in the formulation of experimentally verifiable queries.

SUPPORTING MATERIAL

Supporting Materials and Methods and seven figures are available at [http://www.biophysj.org/biophysj/supplemental/S0006-3495\(17\)31253-5](http://www.biophysj.org/biophysj/supplemental/S0006-3495(17)31253-5).

AUTHOR CONTRIBUTIONS

A.G., L.A.S.-E., and N.L. designed the research. L.A.S.-E., N.L., and T.D.R. performed the research. T.D.R., A.G., and L.A.S.-E. contributed analytic tools. L.A.S.-E. analyzed the data and wrote the manuscript. All authors copy-edited the manuscript.

ACKNOWLEDGMENTS

The authors thank the Center for Integrated Research Computing at the University of Rochester for providing computational resources and technical support. L.A.S.-E. also thanks The American Association of University Women (AAUW) for awarding her an International Fellowship during the 2016–2017 cycle.

This work was supported by grant R01GM095496 (to A.G.) from the National Institutes of Health.

SUPPORTING CITATIONS

References (119–130) appear in the Supporting Material.

REFERENCES

- Palsdottir, H., and C. Hunte. 2004. Lipids in membrane protein structures. *Biochim. Biophys. Acta.* 1666:2–18.
- Vigh, L., P. V. Escrivá, ..., J. L. Harwood. 2005. The significance of lipid composition for membrane activity: new concepts and ways of assessing function. *Prog. Lipid Res.* 44:303–344.
- Gibson, N. J., and M. F. Brown. 1993. Lipid headgroup and acyl chain composition modulate the M1–MII equilibrium of rhodopsin in recombinant membranes. *Biochemistry.* 32:2438–2454.
- Litman, B. J., and D. C. Mitchell. 1996. A role for phospholipid polyunsaturation in modulating membrane protein function. *Lipids.* 31:S193–S197.
- Hashimoto, M., M. S. Hossain, ..., O. Shido. 2001. Effects of docosahexaenoic acid on annular lipid fluidity of the rat bile canalicular plasma membrane. *J. Lipid Res.* 42:1160–1168.
- Valiyaveetil, F. I., Y. Zhou, and R. MacKinnon. 2002. Lipids in the structure, folding, and function of the KcsA K⁺ channel. *Biochemistry.* 41:10771–10777.
- Williamson, I. M., S. J. Alvis, ..., A. G. Lee. 2003. The potassium channel KcsA and its interaction with the lipid bilayer. *Cell. Mol. Life Sci.* 60:1581–1590.
- Gullingsrud, J., and K. Schulten. 2004. Lipid bilayer pressure profiles and mechanosensitive channel gating. *Biophys. J.* 86:3496–3509.
- Lee, A. G. 2003. Lipid-protein interactions in biological membranes: a structural perspective. *Biochim. Biophys. Acta.* 1612:1–40.
- Escrivá, P. V. 2006. Membrane-lipid therapy: a new approach in molecular medicine. *Trends Mol. Med.* 12:34–43.
- de Velasco, P. C., H. R. Mendonça, ..., C. A. Serfaty. 2012. Nutritional restriction of omega-3 fatty acids alters topographical fine tuning and leads to a delay in the critical period in the rodent visual system. *Exp. Neurol.* 234:220–229.
- Lee, A. G. 2004. How lipids affect the activities of integral membrane proteins. *Biochim. Biophys. Acta.* 1666:62–87.
- Nogi, T., I. Fathir, ..., K. Miki. 2000. Crystal structures of photosynthetic reaction center and high-potential iron-sulfur protein from *Thermochromatium tepidum*: thermostability and electron transfer. *Proc. Natl. Acad. Sci. USA.* 97:13561–13566.
- Schlame, M., D. Rua, and M. L. Greenberg. 2000. The biosynthesis and functional role of cardiolipin. *Prog. Lipid Res.* 39:257–288.
- Mouritsen, O. G., and M. Bloom. 1984. Mattress model of lipid-protein interactions in membranes. *Biophys. J.* 46:141–153.
- Fattal, D. R., and A. Ben-Shaul. 1993. A molecular model for lipid-protein interaction in membranes: the role of hydrophobic mismatch. *Biophys. J.* 65:1795–1809.
- Pignataro, M. F., M. M. Dodes-Traian, ..., J. P. F. C. Rossi. 2015. Modulation of plasma membrane Ca²⁺-ATPase by neutral phospholipids: effect of the micelle-vesicle transition and the bilayer thickness. *J. Biol. Chem.* 290:6179–6190.
- Gutierrez, M. G., K. S. Mansfield, and N. Malmstadt. 2016. The functional activity of the human serotonin 5-HT1A receptor is controlled by lipid bilayer composition. *Biophys. J.* 110:2486–2495.
- Brown, M. F. 1994. Modulation of rhodopsin function by properties of the membrane bilayer. *Chem. Phys. Lipids.* 73:159–180.
- Botelho, A. V., N. J. Gibson, ..., M. F. Brown. 2002. Conformational energetics of rhodopsin modulated by nonlamellar-forming lipids. *Biochemistry.* 41:6354–6368.
- Contreras, F.-X., A. M. Ernst, ..., B. Brügger. 2011. Specificity of intramembrane protein-lipid interactions. *Cold Spring Harb. Perspect. Biol.* 3:a004705.
- Yeagle, P. L., J. Young, and D. Rice. 1988. Effects of cholesterol on (Na⁺,K⁺)-ATPase ATP hydrolyzing activity in bovine kidney. *Biochemistry.* 27:6449–6452.

23. Chan, W. K. B., H. Zhang, ..., Y. Zhang. 2015. GLASS: a comprehensive database for experimentally validated GPCR-ligand associations. *Bioinformatics*. 31:3035–3042.
24. Deupi, X., and J. Standfuss. 2011. Structural insights into agonist-induced activation of G-protein-coupled receptors. *Curr. Opin. Struct. Biol.* 21:541–551.
25. Deupi, X., J. Standfuss, and G. Schertler. 2012. Conserved activation pathways in G-protein-coupled receptors. *Biochem. Soc. Trans.* 40:383–388.
26. Sun, L., and R. D. Ye. 2012. Role of G protein-coupled receptors in inflammation. *Acta Pharmacol. Sin.* 33:342–350.
27. Garriga, P., and J. Manyosa. 2002. The eye photoreceptor protein rhodopsin. Structural implications for retinal disease. *FEBS Lett.* 528:17–22.
28. Stone, L. S., and D. C. Molliver. 2009. In search of analgesia: emerging roles of GPCRs in pain. *Mol. Interv.* 9:234–251.
29. Brinks, H. L., and A. D. Eckhart. 2010. Regulation of GPCR signaling in hypertension. *Biochim. Biophys. Acta*. 1802:1268–1275.
30. Overington, J. P., B. Al-Lazikani, and A. L. Hopkins. 2006. How many drug targets are there? *Nat. Rev. Drug Discov.* 5:993–996.
31. Pucadyil, T. J., and A. Chattopadhyay. 2004. Cholesterol modulates ligand binding and G-protein coupling to serotonin^{1A} receptors from bovine hippocampus. *Biochim. Biophys. Acta*. 1663:188–200.
32. Dawaliby, R., C. Trubbia, ..., C. Govaerts. 2016. Allosteric regulation of G protein-coupled receptor activity by phospholipids. *Nat. Chem. Biol.* 12:35–39.
33. Gabhauer, S., and R. A. Böckmann. 2016. Membrane-mediated oligomerization of G protein coupled receptors and its implications for GPCR function. *Front. Physiol.* 7:494.
34. Luchetti, G., R. Sircar, ..., R. Rohatgi. 2016. Cholesterol activates the G-protein coupled receptor smoothened to promote Hedgehog signaling. *eLife*. 5:e20304.
35. Vögler, O., J. Casas, ..., P. V. Escribá. 2004. The Gbetagamma dimer drives the interaction of heterotrimeric Gi proteins with nonlamellar membrane structures. *J. Biol. Chem.* 279:36540–36545.
36. Inagaki, S., R. Ghirlando, ..., R. Grisshammer. 2012. Modulation of the interaction between neurotensin receptor NTS1 and Gq protein by lipid. *J. Mol. Biol.* 417:95–111.
37. Palczewski, K. 2010. Oligomeric forms of G protein-coupled receptors (GPCRs). *Trends Biochem. Sci.* 35:595–600.
38. Goddard, A. D., P. M. Dijkman, ..., A. Watts. 2013. Lipid-dependent GPCR dimerization. *Methods Cell Biol.* 117:341–357.
39. Ghanouni, P., Z. Gryczynski, ..., B. K. Kobilka. 2001. Functionally different agonists induce distinct conformations in the G protein coupling domain of the β₂ adrenergic receptor. *J. Biol. Chem.* 276:24433–24436.
40. Peleg, G., P. Ghanouni, ..., R. N. Zare. 2001. Single-molecule spectroscopy of the β₂ adrenergic receptor: observation of conformational substates in a membrane protein. *Proc. Natl. Acad. Sci. USA*. 98:8469–8474.
41. Kofuku, Y., T. Ueda, ..., I. Shimada. 2012. Efficacy of the β₂ adrenergic receptor is determined by conformational equilibrium in the transmembrane region. *Nat. Commun.* 3:1045.
42. Nygaard, R., Y. Zou, ..., B. K. Kobilka. 2013. The dynamic process of β₂-adrenergic receptor activation. *Cell*. 152:532–542.
43. Maeda, R., M. Hiroshima, ..., Y. Imamoto. 2014. Single-molecule observation of the ligand-induced population shift of rhodopsin, a G-protein-coupled receptor. *Biophys. J.* 106:915–924.
44. Manglik, A., and B. Kobilka. 2014. The role of protein dynamics in GPCR function: insights from the β₂AR and rhodopsin. *Curr. Opin. Cell Biol.* 27:136–143.
45. Leioatts, N., T. D. Romo, ..., A. Grossfield. 2015. Retinal conformation changes rhodopsin's dynamic ensemble. *Biophys. J.* 109:608–617.
46. Hanson, M. A., V. Cherezov, ..., R. C. Stevens. 2008. A specific cholesterol binding site is established by the 2.8 Å structure of the human β₂-adrenergic receptor. *Structure*. 16:897–905.
47. Lee, J. Y., and E. Lyman. 2012. Predictions for cholesterol interaction sites on the A2A adenosine receptor. *J. Am. Chem. Soc.* 134:16512–16515.
48. Manna, M., M. Niemelä, ..., I. Vattulainen. 2016. Mechanism of allosteric regulation of β₂-adrenergic receptor by cholesterol. *eLife*. 5:e18432.
49. Neale, C., H. D. Herce, ..., A. E. García. 2015. Can specific protein-lipid interactions stabilize an active state of the β₂ adrenergic receptor? *Biophys. J.* 109:1652–1662.
50. Han, M., S. O. Smith, and T. P. Sakmar. 1998. Constitutive activation of opsin by mutation of methionine 257 on transmembrane helix 6. *Biochemistry*. 37:8253–8261.
51. Altenbach, C., K. Yang, ..., W. L. Hubbell. 1996. Structural features and light-dependent changes in the cytoplasmic interhelical E-F loop region of rhodopsin: a site-directed spin-labeling study. *Biochemistry*. 35:12470–12478.
52. Choe, H.-W., Y. J. Kim, ..., O. P. Ernst. 2011. Crystal structure of metarhodopsin II. *Nature*. 471:651–655.
53. Parkes, J. H., S. K. Gibson, and P. A. Liebman. 1999. Temperature and pH dependence of the metarhodopsin I-metarhodopsin II equilibrium and the binding of metarhodopsin II to G protein in rod disk membranes. *Biochemistry*. 38:6862–6878.
54. Cooper, A., S. F. Dixon, ..., J. L. Robb. 1987. Mechanism of retinal Schiff base formation and hydrolysis in relation to visual pigment photolysis and regeneration: resonance raman spectroscopy of a tetrahedral carbinolamine intermediate and oxygen-18 labeling of retinal at the metarhodopsin state of photoreceptor membranes. *J. Am. Chem. Soc.* 109:7254–7263.
55. Mason, W. T., R. S. Fager, and E. W. Abrahamson. 1973. Lipid and fatty acid composition of frog photoreceptor outer segments. *Biochemistry*. 12:2147–2150.
56. Albert, A. D., J. E. Young, and Z. Paw. 1998. Phospholipid fatty acyl spatial distribution in bovine rod outer segment disk membranes. *Biochim. Biophys. Acta*. 1368:52–60.
57. Mitchell, D. C., M. Straume, and B. J. Litman. 1992. Role of sn-1-saturated, sn-2-polyunsaturated phospholipids in control of membrane receptor conformational equilibrium: effects of cholesterol and acyl chain unsaturation on the metarhodopsin I in equilibrium with metarhodopsin II equilibrium. *Biochemistry*. 31:662–670.
58. Mitchell, D. C., J. T. Lawrence, and B. J. Litman. 1996. Primary alcohols modulate the activation of the G protein-coupled receptor rhodopsin by a lipid-mediated mechanism. *J. Biol. Chem.* 271:19033–19036.
59. Mitchell, D. C., S.-L. Niu, and B. J. Litman. 2003. DHA-rich phospholipids optimize G-protein-coupled signaling. *J. Pediatr.* 143:S80–S86.
60. Teague, W. E., Jr., O. Soubias, ..., K. Gawrisch. 2013. Elastic properties of polyunsaturated phosphatidylethanolamines influence rhodopsin function. *Faraday Discuss.* 161:383–395, discussion 419–459.
61. Bennett, M. P., and D. C. Mitchell. 2008. Regulation of membrane proteins by dietary lipids: effects of cholesterol and docosahexaenoic acid acyl chain-containing phospholipids on rhodopsin stability and function. *Biophys. J.* 95:1206–1216.
62. Huber, T., K. Rajamoothi, ..., M. F. Brown. 2002. Structure of docosahexaenoic acid-containing phospholipid bilayers as studied by ²H NMR and molecular dynamics simulations. *J. Am. Chem. Soc.* 124:298–309.
63. Feller, S. E., K. Gawrisch, and T. B. Woolf. 2003. Rhodopsin exhibits a preference for solvation by polyunsaturated docosahexaenoic acid. *J. Am. Chem. Soc.* 125:4434–4435.
64. Pitman, M. C., A. Grossfield, ..., S. E. Feller. 2005. Role of cholesterol and polyunsaturated chains in lipid-protein interactions:

- molecular dynamics simulation of rhodopsin in a realistic membrane environment. *J. Am. Chem. Soc.* 127:4576–4577.
65. Soubias, O., and K. Gawrisch. 2005. Probing specific lipid-protein interaction by saturation transfer difference NMR spectroscopy. *J. Am. Chem. Soc.* 127:13110–13111.
 66. Grossfield, A., S. E. Feller, and M. C. Pitman. 2006. Contribution of omega-3 fatty acids to the thermodynamics of membrane protein solvation. *J. Phys. Chem. B.* 110:8907–8909.
 67. Soubias, O., and K. Gawrisch. 2012. The role of the lipid matrix for structure and function of the GPCR rhodopsin. *Biochim. Biophys. Acta.* 1818:234–240.
 68. Soubias, O., and K. Gawrisch. 2007. Docosahexaenoyl chains isomerize on the sub-nanosecond time scale. *J. Am. Chem. Soc.* 129:6678–6679.
 69. Soubias, O., W. E. Teague, and K. Gawrisch. 2006. Evidence for specificity in lipid-rhodopsin interactions. *J. Biol. Chem.* 281:33233–33241.
 70. Soubias, O., W. E. Teague, Jr., ..., K. Gawrisch. 2010. Contribution of membrane elastic energy to rhodopsin function. *Biophys. J.* 99:817–824.
 71. Yau, W. M., W. C. Wimley, ..., S. H. White. 1998. The preference of tryptophan for membrane interfaces. *Biochemistry.* 37:14713–14718.
 72. Okada, T., M. Sugihara, ..., V. Buss. 2004. The retinal conformation and its environment in rhodopsin in light of a new 2.2 Å crystal structure. *J. Mol. Biol.* 342:571–583.
 73. Park, J. H., P. Scheerer, ..., O. P. Ernst. 2008. Crystal structure of the ligand-free G-protein-coupled receptor opsin. *Nature.* 454:183–187.
 74. Grossfield, A., M. C. Pitman, ..., K. Gawrisch. 2008. Internal hydration increases during activation of the G-protein-coupled receptor rhodopsin. *J. Mol. Biol.* 381:478–486.
 75. Lüdeke, S., M. Beck, ..., R. Vogel. 2005. The role of Glu181 in the photoactivation of rhodopsin. *J. Mol. Biol.* 353:345–356.
 76. Shaikh, S. R., M. R. Brzustowicz, ..., S. R. Wassall. 2001. Formation of inverted hexagonal phase in SDPE as observed by solid-state ^{31}P NMR. *Biochem. Biophys. Res. Commun.* 286:758–763.
 77. Teague, W. E., N. L. Fuller, ..., K. Gawrisch. 2002. Polyunsaturated lipids in membrane fusion events. *Cell. Mol. Biol. Lett.* 7:262–264.
 78. Katsaras, J., and T. Gutberlet. 2001. Lipid Bilayers: Structure and Interactions. Springer-Verlag, Berlin, Germany.
 79. Grossfield, A., S. E. Feller, and M. C. Pitman. 2006. A role for direct interactions in the modulation of rhodopsin by omega-3 polyunsaturated lipids. *Proc. Natl. Acad. Sci. USA.* 103:4888–4893.
 80. Hong, C., D. P. Tieleman, and Y. Wang. 2014. Microsecond molecular dynamics simulations of lipid mixing. *Langmuir.* 30:11993–12001.
 81. Woolf, T. B., and B. Roux. 1996. Structure, energetics, and dynamics of lipid-protein interactions: a molecular dynamics study of the gramicidin A channel in a DMPC bilayer. *Proteins.* 24:92–114.
 82. Romo, T. D., N. Leioatts, and A. Grossfield. 2014. Lightweight object oriented structure analysis: tools for building tools to analyze molecular dynamics simulations. *J. Comput. Chem.* 35:2305–2318.
 83. Phillips, J. C., R. Braun, ..., K. Schulten. 2005. Scalable molecular dynamics with NAMD. *J. Comput. Chem.* 26:1781–1802.
 84. MacKerell, A. D., D. Bashford, ..., M. Karplus. 1998. All-atom empirical potential for molecular modeling and dynamics studies of proteins. *J. Phys. Chem. B.* 102:3586–3616.
 85. MacKerell, A. D., Jr., M. Feig, and C. L. Brooks, 3rd. 2004. Extending the treatment of backbone energetics in protein force fields: limitations of gas-phase quantum mechanics in reproducing protein conformational distributions in molecular dynamics simulations. *J. Comput. Chem.* 25:1400–1415.
 86. Klauda, J. B., R. M. Venable, ..., R. W. Pastor. 2010. Update of the CHARMM all-atom additive force field for lipids: validation on six lipid types. *J. Phys. Chem. B.* 114:7830–7843.
 87. Zhu, S., M. F. Brown, and S. E. Feller. 2013. Retinal conformation governs pKa of protonated Schiff base in rhodopsin activation. *J. Am. Chem. Soc.* 135:9391–9398.
 88. Ryckaert, J.-P., G. Ciccotti, and H. J. Berendsen. 1977. Numerical integration of the cartesian equations of motion of a system with constraints: molecular dynamics of *n*-alkanes. *J. Comput. Phys.* 23:327–341.
 89. Essmann, U., L. Perera, ..., L. G. Pedersen. 1995. A smooth particle mesh Ewald method. *J. Chem. Phys.* 103:8577–8593.
 90. Humphrey, W., A. Dalke, and K. Schulten. 1996. VMD: visual molecular dynamics. *J. Mol. Graph.* 14:33–38, 27–28.
 91. Schrödinger, L. L. C., 2015. The PyMOL Molecular Graphics System, Version 1.8.
 92. Carrillo-Tripp, M., and S. E. Feller. 2005. Evidence for a mechanism by which omega-3 polyunsaturated lipids may affect membrane protein function. *Biochemistry.* 44:10164–10169.
 93. Vermeer, L. S., B. L. de Groot, ..., J. Czaplicki. 2007. Acyl chain order parameter profiles in phospholipid bilayers: computation from molecular dynamics simulations and comparison with ^2H NMR experiments. *Eur. Biophys. J.* 36:919–931.
 94. Horn, J. N., T.-C. Kao, and A. Grossfield. 2014. Coarse-grained molecular dynamics provides insight into the interactions of lipids and cholesterol with rhodopsin. *Adv. Exp. Med. Biol.* 796:75–94.
 95. Ballesteros, J. A., and H. Weinstein. 1995. Integrated methods for the construction of three-dimensional models and computational probing of structure-function relations in G protein-coupled receptors. In Receptor Molecular Biology. Elsevier, pp. 366–428.
 96. Pope, A., M. Eilers, ..., S. O. Smith. 2014. Amino acid conservation and interactions in rhodopsin: probing receptor activation by NMR spectroscopy. *Biochim. Biophys. Acta.* 1837:683–693.
 97. Ahuja, S., E. Crocker, ..., S. O. Smith. 2009. Location of the retinal chromophore in the activated state of rhodopsin*. *J. Biol. Chem.* 284:10190–10201.
 98. Franke, R. R., B. König, ..., K. P. Hofmann. 1990. Rhodopsin mutants that bind but fail to activate transducin. *Science.* 250:123–125.
 99. Shi, W., S. Osawa, ..., E. R. Weiss. 1995. Rhodopsin mutants discriminate sites important for the activation of rhodopsin kinase and G_i. *J. Biol. Chem.* 270:2112–2119.
 100. Acharya, S., Y. Saad, and S. S. Karnik. 1997. Transducin- α C-terminal peptide binding site consists of C-D and E-F loops of rhodopsin. *J. Biol. Chem.* 272:6519–6524.
 101. Kissilev, O. G., M. A. Downs, ..., P. A. Hargrave. 2004. Conformational changes in the phosphorylated C-terminal domain of rhodopsin during rhodopsin arrestin interactions. *J. Biol. Chem.* 279:51203–51207.
 102. Jones Brunette, A. M., A. Sinha, ..., D. L. Farrens. 2016. Evidence that the rhodopsin kinase (GRK1) N-terminus and the transducin G α C-terminus interact with the same “hydrophobic patch” on rhodopsin TM5. *Biochemistry.* 55:3123–3135.
 103. Cherezov, V., D. M. Rosenbaum, ..., R. C. Stevens. 2007. High-resolution crystal structure of an engineered human β_2 -adrenergic G protein-coupled receptor. *Science.* 318:1258–1265.
 104. Rosenbaum, D. M., C. Zhang, ..., B. K. Kobilka. 2011. Structure and function of an irreversible agonist- β_2 adrenoceptor complex. *Nature.* 469:236–240.
 105. Dror, R. O., D. H. Arlow, ..., D. E. Shaw. 2011. Activation mechanism of the β_2 -adrenergic receptor. *Proc. Natl. Acad. Sci. USA.* 108:18684–18689.
 106. Soubias, O., S.-L. Niu, ..., K. Gawrisch. 2008. Lipid-rhodopsin hydrophobic mismatch alters rhodopsin helical content. *J. Am. Chem. Soc.* 130:12465–12471.
 107. Polozova, A., and B. J. Litman. 2000. Cholesterol dependent recruitment of di22:6-PC by a G protein-coupled receptor into lateral domains. *Biophys. J.* 79:2632–2643.
 108. Gawrisch, K., O. Soubias, and M. Mihailescu. 2008. Insights from biophysical studies on the role of polyunsaturated fatty acids for

- function of G-protein coupled membrane receptors. *Prostaglandins Leukot. Essent. Fatty Acids.* 79:131–134.
109. Cooper, A. 1979. Energy uptake in the first step of visual excitation. *Nature.* 282:531–533.
 110. Flyvbjerg, H., F. Jülicher, ..., F. David. 2002. Physics of Bio-Molecules and Cells: Les Houches Session LXXV, 2–27 July 2001,. Springer-Verlag, Berlin, Germany.
 111. Dilger, J., L. Musbat, ..., Y. Toker. 2015. Direct measurement of the isomerization barrier of the isolated retinal chromophore. *Angew. Chem. Int. Ed. Engl.* 54:4748–4752.
 112. Krishna, A. G., S. T. Menon, ..., T. P. Sakmar. 2002. Evidence that helix 8 of rhodopsin acts as a membrane-dependent conformational switch. *Biochemistry.* 41:8298–8309.
 113. Li, J., P. C. Edwards, ..., G. F. X. Schertler. 2004. Structure of bovine rhodopsin in a trigonal crystal form. *J. Mol. Biol.* 343:1409–1438.
 114. Piscitelli, C. L., T. E. Angel, ..., C. M. Lawrence. 2006. Equilibrium between metarhodopsin-I and metarhodopsin-II is dependent on the conformation of the third cytoplasmic loop. *J. Biol. Chem.* 281:6813–6825.
 115. Schertler, G. F. X. 2005. Structure of rhodopsin and the metarhodopsin I photointermediate. *Curr. Opin. Struct. Biol.* 15:408–415.
 116. Kobilka, B. K. 2007. G protein coupled receptor structure and activation. *Biochim. Biophys. Acta.* 1768:794–807.
 117. Elgeti, M., A. S. Rose, ..., M. Heck. 2013. Precision vs flexibility in GPCR signaling. *J. Am. Chem. Soc.* 135:12305–12312.
 118. Baldwin, P. A., and W. L. Hubbell. 1985. Effects of lipid environment on the light-induced conformational changes of rhodopsin. 1. Absence of metarhodopsin II production in dimyristoylphosphatidylcholine recombinant membranes. *Biochemistry.* 24:2624–2632.
 119. Klauda, J. B., V. Monje, ..., W. Im. 2012. Improving the CHARMM force field for polyunsaturated fatty acid chains. *J. Phys. Chem. B.* 116:9424–9431.
 120. Venable, R. M., F. L. H. Brown, and R. W. Pastor. 2015. Mechanical properties of lipid bilayers from molecular dynamics simulation. *Chem. Phys. Lipids.* 192:60–74.
 121. Flyvbjerg, H., and H. G. Petersen. 1989. Error estimates on averages of correlated data. *J. Chem. Phys.* 91:461–466.
 122. Grossfield, A., and D. M. Zuckerman. 2009. Quantifying uncertainty and sampling quality in biomolecular simulations. *Annu. Rep. Comput. Chem.* 5:23–48.
 123. Barber, C. B., D. P. Dobkin, and H. Huhdanpaa. 1996. The Quickhull algorithm for convex hulls. *ACM Trans. Math. Softw.* 22:469–483.
 124. Oliphant, T. E. 2007. Python for scientific computing. *Comput. Sci. Eng.* 9:10–20.
 125. Lindahl, E., and O. Edholm. 2000. Mesoscopic undulations and thickness fluctuations in lipid bilayers from molecular dynamics simulations. *Biophys. J.* 79:426–433.
 126. Sonne, J., F. Y. Hansen, and G. H. Peters. 2005. Methodological problems in pressure profile calculations for lipid bilayers. *J. Chem. Phys.* 122:124903.
 127. Horn, J. N., T. D. Romo, and A. Grossfield. 2013. Simulating the mechanism of antimicrobial lipopeptides with all-atom molecular dynamics. *Biochemistry.* 52:5604–5610.
 128. Leioatts, N., B. Mertz, ..., M. F. Brown. 2014. Retinal ligand mobility explains internal hydration and reconciles active rhodopsin structures. *Biochemistry.* 53:376–385.
 129. Kabsch, W., and C. Sander. 1983. Dictionary of protein secondary structure: pattern recognition of hydrogen-bonded and geometrical features. *Biopolymers.* 22:2577–2637.
 130. Touw, W. G., C. Baakman, ..., G. Vriend. 2015. A series of PDB-related databanks for everyday needs. *Nucleic Acids Res.* 43:D364–D368.

Supplemental Information

Lipids Alter Rhodopsin Function via Ligand-like and Solvent-like Interactions

Leslie A. Salas-Estrada, Nicholas Leioatts, Tod D. Romo, and Alan Grossfield

S1 Neat SDPE membranes

We started the preliminary and production runs for these simulations with the original CHARMM36 force field for lipids(1), a couple of years after its release. Our initial testing suggested that applying a surface tension was still necessary to obtain the area per lipid extrapolated from experiments for SDPE membranes(2).

This discrepancy between experimentally measured observables and those computed from MD simulations for bilayers with polyunsaturated lipids was also noticed by other groups and the force field was improved later on for polyunsaturated phospholipids(3, 4). However, at that point, we had already invested significant computational effort with the previous force field and chose to continue with it for the sake of consistency.

Fig. S1a shows the behavior of pure SDPE systems under different surface tensions: 5 dyn/cm (green), 7.5 dyn/cm (cyan), 10 dyn/cm (purple), 15 dyn/cm (black), 20 dyn/cm (orange), 25 dyn/cm (blue), 28 dyn/cm (gray), 30 dyn/cm (light brown), 35 dyn/cm (pink) and 40 dyn/cm (red). These trajectories were run under the same simulation conditions as the rhodopsin-containing systems.

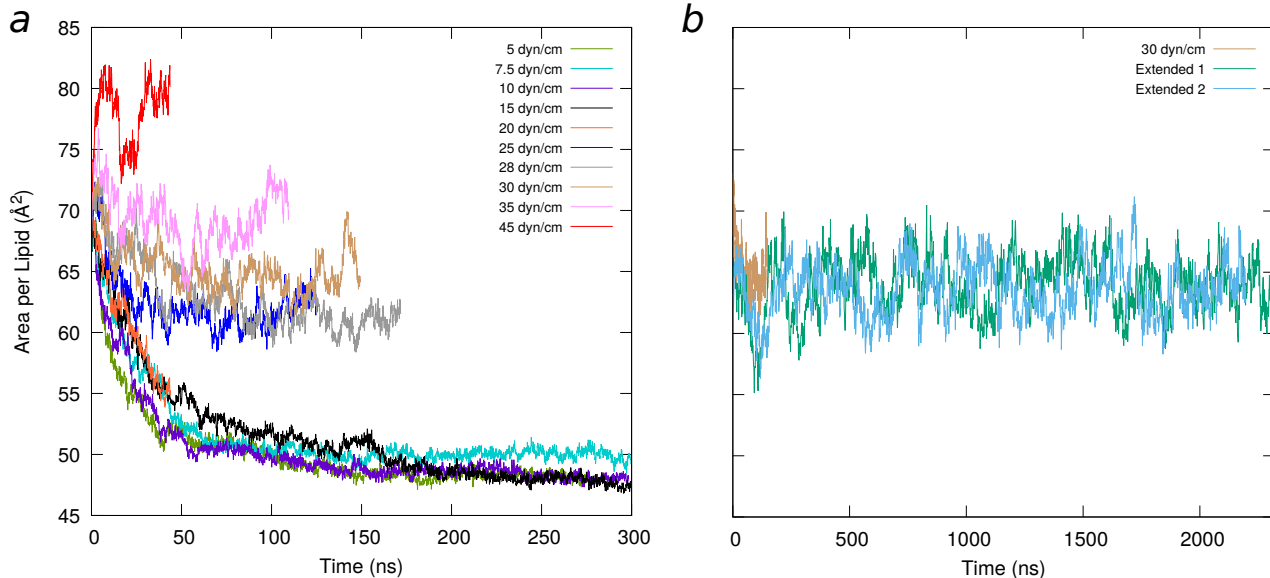


Figure S1: Area per lipid of neat SDPE membranes. *a)* Area per lipid of pure SDPE bilayers simulated with different surface tensions: 5 dyn/cm (green), 7.5 dyn/cm (cyan), 10 dyn/cm (purple), 15 dyn/cm (black), 20 dyn/cm (orange), 25 dyn/cm (blue), 28 dyn/cm (gray), 30 dyn/cm (light brown), 35 dyn/cm (pink) and 40 dyn/cm (red). *b)* Extended simulations of the system in *a*) with a surface tension of 30 dyn/cm (light brown).

Our simulations suggest that a surface tension of 30 dyn/cm produces an area per lipid for SDPE that is within error of that reported by other groups(2, 4). Fig. S1b shows two microsecond-scale trajectories under a 30 dyn/cm surface tension. Their average area per lipid and standard deviation are $(63.84 \pm 2.42) \text{ \AA}^2$ (Extended 1; green) and $(63.58 \pm 2.24) \text{ \AA}^2$ (Extended 2; blue). We calculated the standard error of these averages using the block averaging algorithm described by Flyvbjerg and Petersen(4–6). The resulting estimates are 0.33 \AA^2 and 0.42 \AA^2 , respectively.

S2 Cross-sectional area

We computed the average cross-sectional area profile of rhodopsin from the dark state, Meta I and Meta II trajectories at 100 ps time resolution. We verified that excluding all hydrogen atoms from the calculation did not significantly change the answer by comparing calculations with and without hydrogens for the first 250 ns. Thus, we carried out the calculation only with heavy atoms to reduce the computation time. For every frame of a trajectory, the simulation cell was sliced into 80 bins along the membrane normal (z-axis) so that each bin had a z-width of $\sim 1 \text{ \AA}$. Then, the heavy atoms in each slice were partitioned using a Voronoi decomposition(7, 8). To avoid artifacts from the edges of the periodic box at this point, we used a padding of 15 \AA (2-3 layers of dummy atoms) around the atoms of interest. The reported area of the receptor in each z-slice for a given trajectory frame was obtained by computing the smallest convex hull delimiting the heavy atoms of the transmembrane segment of the protein. Finally, the cross-sectional areas for each z-bin were averaged over time along each trajectory. The cross-sectional areas presented in Fig. 1 in the main text and Fig. S2 are the average of six independent simulations per protein state. Error bars indicate the mean \pm SE, computed by treating each simulation as a single data point. These types of calculations have been automated as an analysis tool, `area_profile`, that is part of the Voronoi package of LOOS.

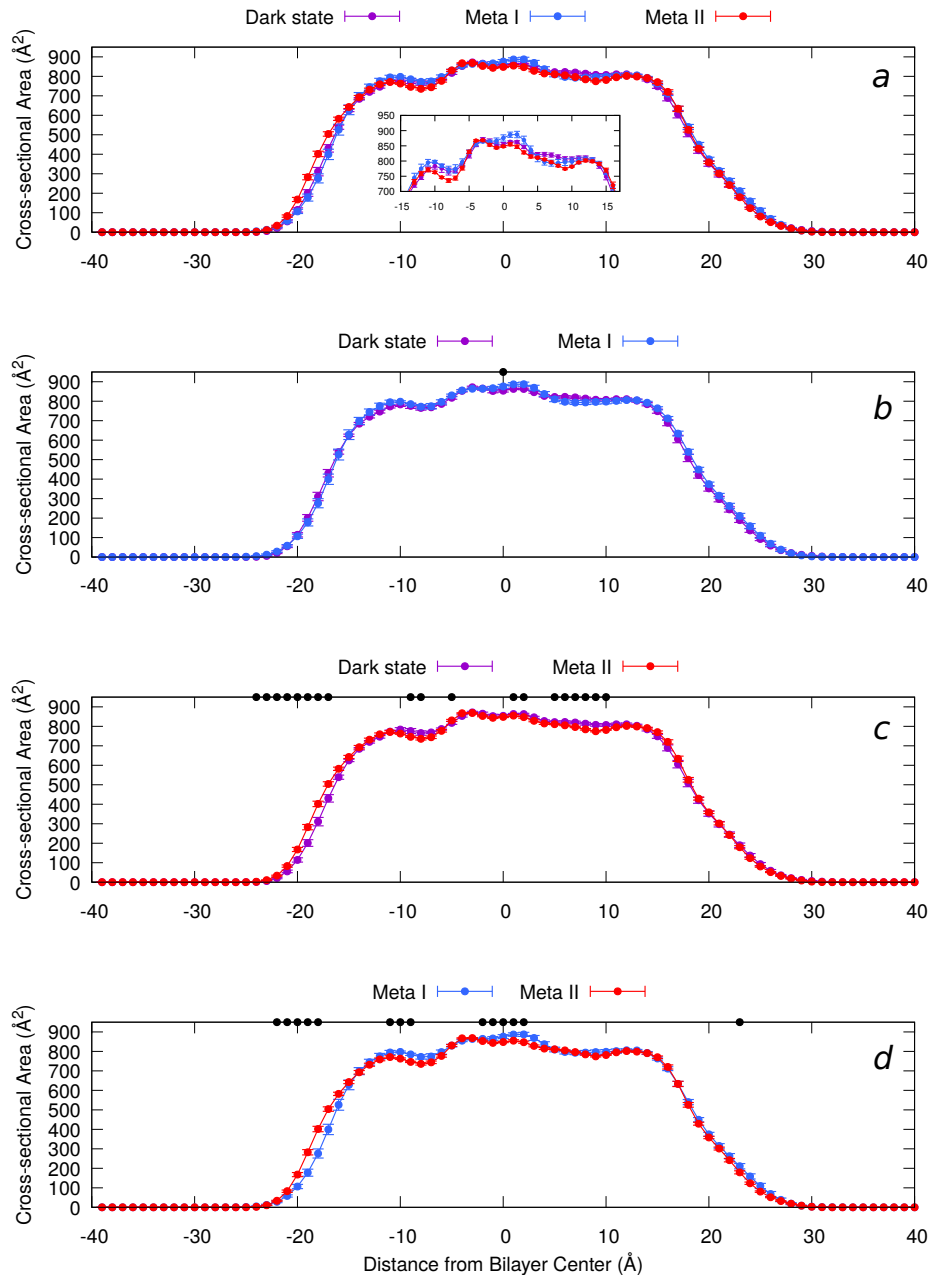


Figure S2: Average cross-sectional area profiles of rhodopsin states. For each frame in a trajectory we took $\sim 1 \text{ \AA}$ slices along the membrane normal. Then, for each slice, we performed a Voronoi analysis to find the smallest convex envelope enclosing every transmembrane heavy atom of the protein in that plane (i.e. its cross-sectional area). We then averaged these areas over the length of the trajectory. The resulting profiles were additionally averaged over six replicates of each protein state as shown in *a*) where the inset corresponds to the cross-sectional areas of the $-15 < z < 15$ region, with the y-axis scaled up. To find statistically significant differences among protein states, we performed a *t*-test for each pairwise comparison: *b*) dark state versus Meta I; *c*) dark state versus Meta II; and *d*) Meta I versus Meta II. Significantly different cross-sectional areas along the bilayer normal with p -values < 0.05 are indicated by black dots at the top of each plot.

S3 Molecular order parameters

We employed LOOS tool `dibmops` to examine the average structure and the disorder of the membrane lipids in our dark state, Meta I and Meta II systems. `dibmops` was written as a whole-chain analog to C-D bond order parameters of perdeuterated lipid tails (S_{CD}), which are customarily measured from ^2H quadripolar splittings in solid-state NMR and report on the average orientations of C-D bonds with respect to the membrane normal (θ_{CD}),

$$S_{CD} = -\frac{1}{2} \langle 3 \cos^2 \theta_{CD} - 1 \rangle \quad (1)$$

The algorithm computes the principal axes of an acyl chain and uses the orientations of the second and third principal axes with respect to the membrane normal, in analogy to θ_{CD} . The first principal axis captures the tilt of the chain, while the other two define a plane that is orthogonal to it. We refer to the quantity computed from the orientations of the second and third principal axes of an acyl chain with respect to the membrane normal using Eq. 1 as molecular order parameters(9). For these calculations, the protein is centered at the origin. For every time point in a trajectory, the molecular order parameters of DHA and STEA acyl chains were binned as a function of distance from the protein centroid. Fig. 2a in the main text shows the average distance-based distributions of molecular order parameters of six simulations per protein state, with error bars corresponding to the mean \pm SE, treating each trajectory as a single measurement.

We used a pairwise t -test to find statistically significant differences among the average STEA molecular order parameters distributions of the dark, Meta I and Meta II states (see Fig. S3). We observe statistically significant differences at short and long distances from the protein centroid. At 11-15 Å from the centroid of the protein, the inactive distributions (dark and Meta I) are not significantly different. Conversely, the active distribution (Meta II) is significantly different from the inactive ones in this area of the membrane. The differences observed among the three distributions at 25-35 Å from the protein centroid, although small, are also significantly different, indicating that even at these long-ranges the protein can still alter the structure of the membrane. These effects, however, are expected to decay at larger distances from the receptor.

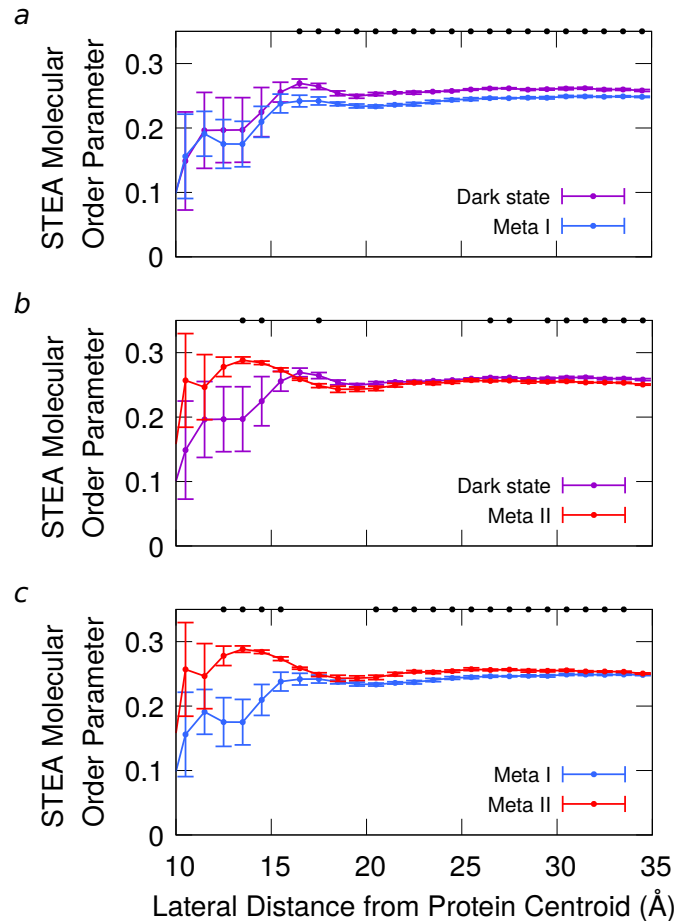


Figure S3: Average STEA molecular order parameters distributions in different rhodopsin states. We computed the average STEA molecular order parameters as a function of distance from the protein centroid in each trajectory as detailed in the main text (see Fig. 2a). To obtain average distributions for the dark, Meta I and Meta II states, we averaged six trajectories per protein state. Error bars indicate the mean \pm SE. To find statistically significant differences among these protein states, we performed a *t*-test for each pairwise comparison, treating each trajectory of a given protein state as a single measurement: *a)* dark state versus Meta I; *b)* dark state versus Meta II; and *c)* Meta I versus Meta II. Significantly different STEA molecular order parameters with p-values < 0.05 are indicated by black dots at the top of each plot.

S4 Acyl chain end-to-end distance

For every time point in a trajectory, the end-to-end distance of each STEA acyl chain (C1-C18 distance) was histogrammed as a function of distance from the protein centroid using the LOOS framework. Fig. 2b in the main text shows the distance-based distribution of STEA end-to-end distances averaged over six simulations per protein state. Error bars indicated the mean \pm SE, computed by treating each simulation as a single data point.

S5 Lipid-binding lifetimes

To detect instances of lipid tails penetrating the protein core along a trajectory, we first centered the membrane at the origin. Then, at every time point, we sliced the system along the membrane normal (z-axis) from its center into 10 bins of approximately 3.4 Å thickness. Using only the backbone atoms of the protein, we computed the centroid of each protein helix within a given slice and found the smallest convex hull delimiting all the centroids (see Fig. 3 in the main text). Because the surface of the protein is not uniform as a function of membrane depth, this algorithm allows us to recalculate it for each slice so that helix kinks and tilts are properly captured. We chose \sim 3.4 Å as the bin z-width in order to guarantee that multiple atoms from every protein helix were present in every slice (a minimum of 3 helix centroids is needed to compute a convex hull), while still picking up changes in the protein surface. Finally, the position of each atom in a lipid tail was monitored to determine whether it was inside or outside the protein core. If, at a given time point, one or more lipid atoms were found inside a convex hull corresponding to any of the slices, the lipid tail was considered to be inside. To find the distribution of lipid residence times inside the protein, we histogrammed the number of time points in which each lipid tail was found inside the protein along a trajectory. Instances of lipid tails staying inside for more than 1500 ns were added together. The results obtained from the analysis of lipid-binding events were not sensitive to the precise definition of short-lived and long-lived events. Figs. S4 and S5 show the aggregate distributions of DHA and STEA residence times computed from six independent simulations per protein state. This algorithm has been implemented as a trajectory analysis tool, `inside_helices`, and is now part of the PyLOOS package of LOOS. The present implementation can detect any user-specified probe (e.g. lipid headgroups) moving to the inside of a helical protein.

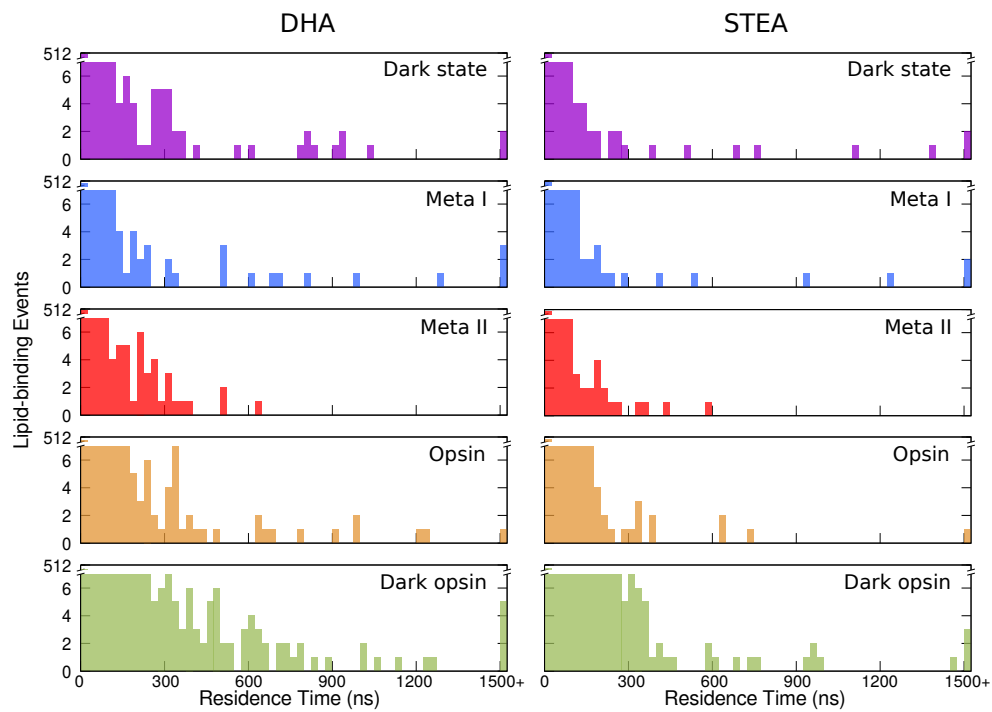


Figure S4: Residence times of phospholipid acyl tails inside rhodopsin. Distributions of the residence times of DHA (*left column*) and STEA (*right column*) binding events by protein state. These distributions were computed from the full trajectories (including the first 500 ns of the simulation). Binding events longer than 1500 ns are grouped together.

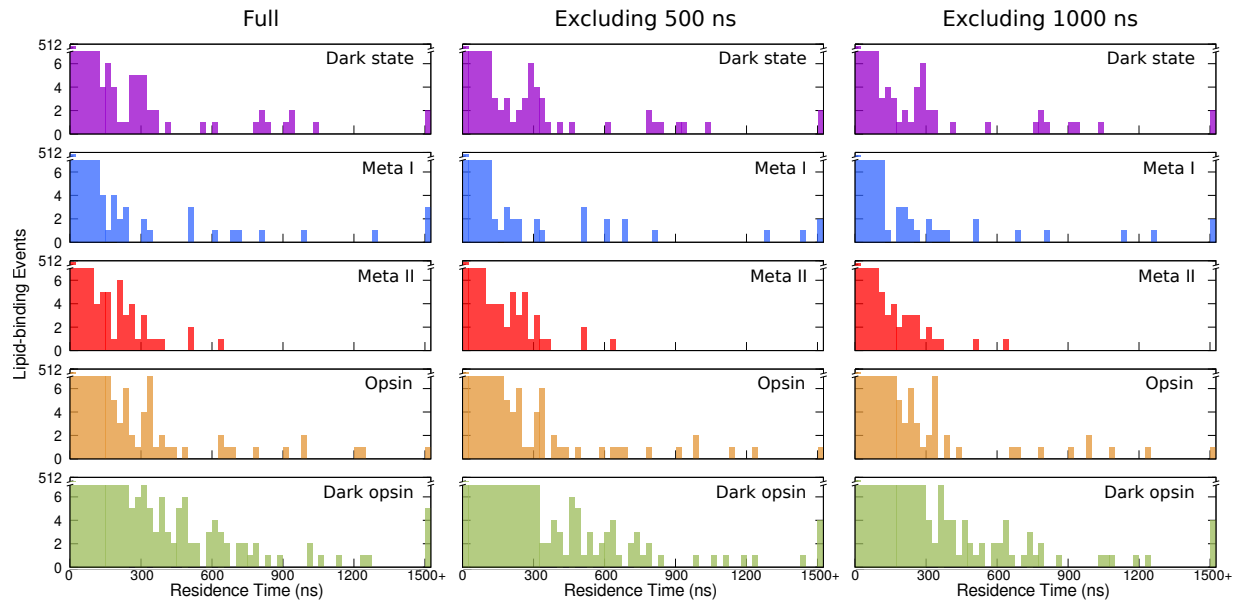


Figure S5: Residence times of DHA acyl chains inside rhodopsin. Distributions of the residence times of DHA-binding events by protein state computed using the full trajectories (*left column*), excluding the first 500 ns (*middle column*) and excluding the first microsecond (*right column*). Binding events longer than 1500 ns are grouped together.

S6 Lipid occupancies

We used the LOOS framework to monitor protein-lipid contacts in our systems. A contact was defined as one or more lipid heavy atoms being within 6 Å of the centroid of a protein side chain. For a given trajectory, we computed the fraction of time that each protein residue spent in contact with one or more lipid molecules; we refer to this quantity as lipid occupancy. Then, we compared the lipid occupancies for individual residues across the different protein states, and used a *t*-test to identify those residues whose occupancy changes are unlikely to be random. To do this, we employed our six simulations per protein state as single measurements and calculated a p-value for each protein residue, comparing two protein states at a time. Figs. 4 and S6 show protein residues with p-values < 0.05.

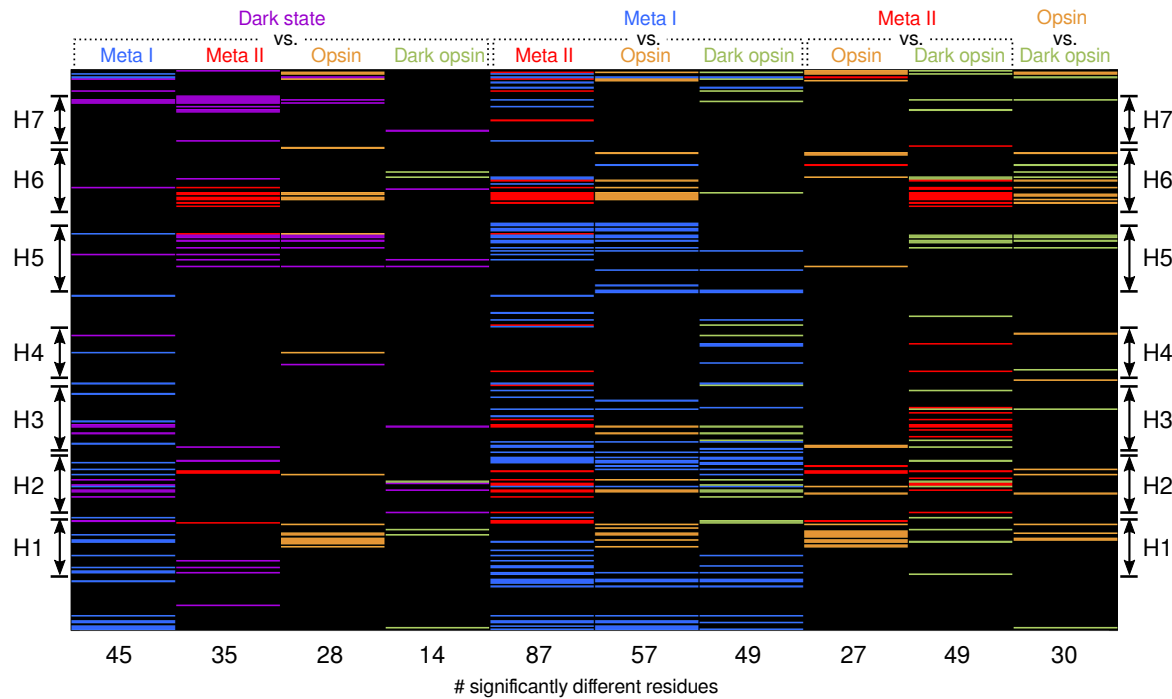


Figure S6: Protein residues differentially occupied by DHA in rhodopsin protein states. To calculate the lipid occupancy of a protein residue, we defined a protein-lipid contact in the following way. First, we computed the centroid of each protein side chain; then, we calculated the distance between these centroids to every heavy atom in a DHA acyl tail to find the minimum distance between the protein residue and a lipid molecule. A protein residue was considered to be in contact with a DHA chain if the minimum distance between them was $< 6 \text{ \AA}$. For each of the six replicates per protein state, we found the fraction of simulation time that each protein residue was in contact with a DHA molecule and divided this quantity over the length of the trajectory. Using these results, we then performed a *t*-test to find which residues were significantly differently occupied between different protein states, comparing them two at a time. Every column in the occupancy matrix represents one of these comparisons; each row corresponds to a protein residue. The transmembrane helices of the protein (H1-H7) are indicated on the sides of the occupancy matrix to guide the eye. For every comparison, each protein residue is presented with the color of the protein state in which the highest occupancy was observed. For example, the first column compares the DHA occupancies of the dark and Meta I trajectories. Every protein residue colored purple has a higher occupancy in the dark state trajectories than in Meta I. Equivalently, every protein residue colored blue has a higher occupancy in the Meta I trajectories than in the dark state. At the bottom, we indicate the number of residues with significantly different occupancies found in each comparison. H: helix.

S7 Retinal methyl orientations

In analogy to ^2H solid-state NMR experiments measuring the orientation of individually deuterated methyl groups in retinal(10, 11), we tracked the orientations of the C5-, C9- and C13-methyls using the LOOS framework. At every time point in a trajectory, we computed the dot product between the membrane normal and vectors defined by the coordinates of atom pairs C5-C18, C19-C9 and C20-C13, as depicted in Fig. 6 in the main text. The resulting time series (e.g. Fig. 5c-e) were also histogrammed into 40 bins, with the area under the curve normalized to 1. Fig. 6 shows the orientation distributions of the three methyl groups averaged over six independent dark state simulations. Error bars indicate the mean \pm SE, treating each simulation as a single data point.

S8 F212^{5.47} χ_1 rotamer and DHA distance

We computed the χ_1 rotamer of F212^{5.47} side chain as a function of time using LOOS tool `rotamer`, as shown in Fig. 5b in the main text. In addition, we employed `interdist` (also included in LOOS) to monitor the minimum distance between F212^{5.47} and DHA acyl chains (e.g. Fig. 5a).

S9 Secondary structure assignments

We used `mkdssp`(12, 13) to compute the secondary structure assignments of residues Q225^{5.60}-V250^{6.33}. This application employs Kabsch and Sander's algorithm, DSSP, to compute protein secondary structure assignments based on tertiary structure(12, 13). Because `mkdssp` takes a single PDB as input, we wrote a Python wrapper around it using LOOS that iterates over each frame of a given trajectory and produces a time series with the secondary structure assignments of interest. This script is available upon request. For clarity, we simplified the eight types of secondary structures defined by DSSP into two broader categories: 1) *Helix* (α -helices, 3_{10} -helices and π -helices) and 2) *Other* (residues in isolated β -bridges, extended strands, hydrogen-bonded turns and bends). We have used this classification to monitor changes in the secondary structure of the receptor as show in Fig. 7a in the main text and Fig. S7.

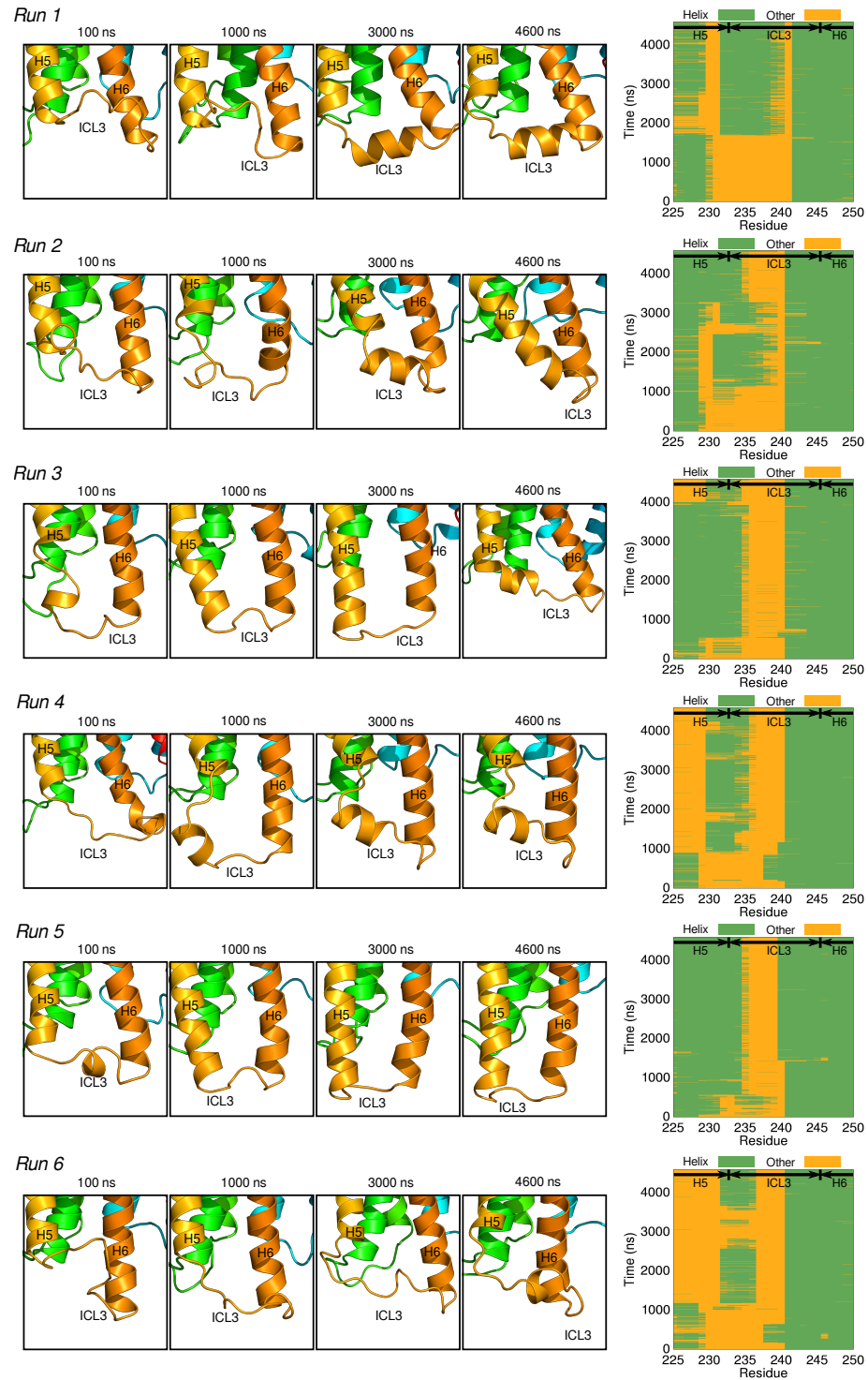


Figure S7: Time evolution of ICL3 in dark state rhodopsin trajectories. Snapshots of ICL3 from the six dark state trajectories at 100 ns, 1000 ns, 3000 ns and 4600 ns. The loop becomes partially structured in all trajectories at different time points. The time evolution of the secondary structure assignments of protein residues Q225^{5,60}-V250^{6,33} is shown for each simulation on the right. H5: helix 5; ICL3: intracellular loop 3; H6: helix 6.

S10 E232^{5.67}-K248^{6.31} distance

The interatomic distance between the δ -carboxyl oxygens of E232^{5.67} and the ϵ -amino nitrogen of K248^{6.31} was calculated using LOOS tool `interdist`. At every time point in a trajectory, the tool computes the minimum distance between the specified sets of atoms. Fig. 7b in the main text shows the interatomic distance between E232^{5.67} and K248^{6.31} as a function of time in one of the dark state trajectories.

S11 E232^{5.67} fraction of contacts

The fraction of contacts of E232^{5.67} was computed using LOOS tool `fcontacts`. For this calculation, all atoms within hydrogen-bonding distance (3.2 Å) of the δ -carboxyl oxygens of E232^{5.67} were considered as contacts and normalized to 1 at a every trajectory time point. Then, the fraction of these contacts corresponding to interatomic interactions with the ϵ -amino nitrogen of K248^{6.31} or any PE nitrogens within the cutoff distance was monitored over time as shown in Fig. 7c in the main text.

Supporting References

1. Klauda, J. B., R. M. Venable, J. A. Freites, J. W. O'Connor, D. J. Tobias, C. Mondragon-Ramirez, I. Vorobyov, A. D. MacKerell, Jr, and R. W. Pastor, 2010. Update of the CHARMM all-atom additive force field for lipids: validation on six lipid types. *J. Phys. Chem. B* 114:7830–7843. <http://dx.doi.org/10.1021/jp101759q>.
2. Soubias, O., W. E. Teague, Jr, K. G. Hines, D. C. Mitchell, and K. Gawrisch, 2010. Contribution of membrane elastic energy to rhodopsin function. *Biophys. J.* 99:817–824. <http://dx.doi.org/10.1016/j.bpj.2010.04.068>.
3. Klauda, J. B., V. Monje, T. Kim, and W. Im, 2012. Improving the CHARMM force field for polyunsaturated fatty acid chains. *J. Phys. Chem. B* 116:9424–9431.
4. Venable, R. M., F. L. H. Brown, and R. W. Pastor, 2015. Mechanical properties of lipid bilayers from molecular dynamics simulation. *Chem. Phys. Lipids* 192:60–74.
5. Flyvbjerg, H., and H. G. Petersen, 1989. Error estimates on averages of correlated data. *J. Chem. Phys.* 91:461–466.
6. Grossfield, A., and D. M. Zuckerman, 2009. Quantifying uncertainty and sampling quality in biomolecular simulations. *Annu. Rep. Comput. Chem.* 5:23–48.
7. Barber, C. B., D. P. Dobkin, and H. Huhdanpaa, 1996. The Quickhull algorithm for convex hulls. *ACM Trans. Math. Softw.* 22:469–483.
8. Oliphant, T. E., 2007. Python for Scientific Computing. *Comput. Sci. Eng.* 9:10–20.
9. Horn, J. N., T. D. Romo, and A. Grossfield, 2013. Simulating the mechanism of antimicrobial lipopeptides with all-atom molecular dynamics. *Biochemistry* 52:5604–5610.
10. Leioatts, N., B. Mertz, K. Martínez-Mayorga, T. D. Romo, M. C. Pitman, S. E. Feller, A. Grossfield, and M. F. Brown, 2014. Retinal ligand mobility explains internal hydration and reconciles active rhodopsin structures. *Biochemistry* 53:376–385. <http://dx.doi.org/10.1021/bi4013947>.
11. Leioatts, N., T. D. Romo, S. A. Danial, and A. Grossfield, 2015. Retinal Conformation Changes Rhodopsin's Dynamic Ensemble. *Biophys. J.* 109:608–617. <http://dx.doi.org/10.1016/j.bpj.2015.06.046>.
12. Kabsch, W., and C. Sander, 1983. Dictionary of protein secondary structure: pattern recognition of hydrogen-bonded and geometrical features. *Biopolymers* 22:2577–2637. <http://dx.doi.org/10.1002/bip.360221211>.
13. Touw, W. G., C. Baakman, J. Black, T. A. H. te Beek, E. Krieger, R. P. Joosten, and G. Vriend, 2015. A series of PDB-related databanks for everyday needs. *Nucleic Acids Res.* 43:D364–D368. <http://dx.doi.org/10.1093/nar/gku1028>.